

SEISMIC ATTRIBUTE ANALYSIS USING HIGHER ORDER STATISTICS

A Thesis

by

JANELLE GREENIDGE

Submitted to the Office of Graduate Studies of
Texas A&M University
in partial fulfillment of the requirements for the degree of

MASTER OF SCIENCE

August 2008

Major Subject: Geophysics

SEISMIC ATTRIBUTE ANALYSIS USING HIGHER ORDER STATISTICS

A Thesis

by

JANELLE GREENIDGE

Submitted to the Office of Graduate Studies of
Texas A&M University
in partial fulfillment of the requirements for the degree of

MASTER OF SCIENCE

Approved by:

Chair of Committee,
Committee Members,

Head of Department,

Luc T. Ikelle
John R. Hopper
Daulat D. Mamora
Andreas K. Kronenberg

August 2008

Major Subject: Geophysics

ABSTRACT

Seismic Attribute Analysis Using Higher Order Statistics. (August 2008)

Janelle Greenidge, B.S., University of the West Indies

Chair of Advisory Committee: Dr. Luc T. Ikelle

Seismic data processing depends on mathematical and statistical tools such as convolution, crosscorrelation and stack that employ second-order statistics (SOS). Seismic signals are non-Gaussian and therefore contain information beyond SOS. One of the modern challenges of seismic data processing is reformulating algorithms e.g. migration, to utilize the extra higher order statistics (HOS) information in seismic data.

The migration algorithm has two key components: the moveout correction, which corresponds to the crosscorrelation of the migration operator with the data at zero lag and the stack of the moveout-corrected data. This study reformulated the standard migration algorithm to handle the HOS information by improving the stack component, having assumed that the moveout correction is accurate. The reformulated migration algorithm outputs not only the standard form of stack, but also the variance, skewness and kurtosis of moveout-corrected data.

The mean (stack) of the moveout-corrected data in this new concept is equivalent to the migration currently performed in industry. The variance of moveout-corrected data is one of the new outputs obtained from the reformulation. Though it characterizes SOS information, it is not one of the outputs of standard migration. In cases where the seismic amplitude variation with offset (AVO) response is linear, a single algorithm that

outputs mean (stack) and variance combines both the standard AVO analysis and migration, thereby significantly improving the cost of seismic data processing. Furthermore, this single algorithm improves the resolution of seismic imaging, since it does not require an explicit knowledge of reflection angles to retrieve AVO information.

In the reformulation, HOS information is captured by the skewness and kurtosis of moveout-corrected data. These two outputs characterize nonlinear AVO response and non-Gaussian noise (symmetric and nonsymmetric) that may be contained in the data. Skewness characterizes nonsymmetric, non-Gaussian noise, whereas kurtosis characterizes symmetric, non-Gaussian noise. These outputs also characterize any errors associated with moveout corrections.

While classical seismic data processing provides a single output, HOS-related processing outputs three extra parameters i.e. the variance, skewness, and kurtosis. These parameters can better characterize geological formations and improve the accuracy of the seismic data processing performed before the application of the reformulated migration algorithm.

DEDICATION

To my beloved mom and dad, for your love, wisdom and support

ACKNOWLEDGEMENTS

I would like to take this opportunity to give my sincere thanks to my academic advisor and the Chair of my Graduate Committee, Dr. Luc Ikelle, for his teaching and support throughout my research. His availability and timely guidance were fundamental to the completion of my program. I am extremely grateful to my other Graduate Committee members, Dr. John Hopper and Dr. Daulat Mamora, for their advice, insightful comments and willingness to share their valuable time during my research period.

My appreciation also goes out to the sponsors of the CASP project, whose resources have made this and other research possible, and to fellow CASP members for their assistance, suggestions and technical support.

Thanks also to the Government of Trinidad and Tobago for rewarding me a scholarship to pursue this degree. Their funding and support during my time at Texas A&M were greatly appreciated.

I wish to extend my gratitude to my family and friends for their unconditional love, patience and support throughout my graduate studies at Texas A&M. Their devotion has been very instrumental in my ability to complete this thesis successfully.

Most importantly, I give my thanks to God, with whom all things are possible.

TABLE OF CONTENTS

	Page
ABSTRACT.....	iii
DEDICATION.....	v
ACKNOWLEDGEMENTS.....	vi
TABLE OF CONTENTS.....	vii
LIST OF TABLES.....	ix
LIST OF FIGURES.....	x
 CHAPTER	
I INTRODUCTION.....	1
II SOME BACKGROUND OF STATISTICAL AVERAGES OF NON-GAUSSIAN RANDOM VARIABLES.....	13
Introduction.....	13
Moments and Cumulants.....	14
Non-Gaussian Probability Distribution.....	16
III HOS AND AVO SEISMIC DATA.....	19
Introduction.....	19
Examples of the Effect of Noise on CMP AVA Seismic Data.....	21
Analysis of Results.....	21
IV ANALYSIS OF HOS MIGRATION THROUGH ONE-DIMENSIONAL GEOLOGICAL MODELS.....	34
Formulation of the HOS Migration Algorithm.....	34
Description of Model.....	35
Examples of HOS Migration.....	38
Analysis of Results.....	38
V SUMMARY AND CONCLUSIONS.....	44

	Page
REFERENCES.....	46
APPENDIX A.....	47
VITA.....	52

LIST OF TABLES

TABLE		Page
2.1	First four orders of cumulants.....	15
2.2	Relation between the first five orders of moments and cumulants.....	16
2.3	First four moments and cumulants of the Gaussian, Laplace, Uniform and Rayleigh distributions.....	18
3.1	Statistical averages of AVO seismic data for different types and variances of additive noise presented in Figures 3.2 to 3.9.....	30
4.1	Output parameters of HOS migration.....	35
4.2	Parameters defining the geological model used for analysis of the new HOS migration algorithm.....	37

LIST OF FIGURES

FIGURE	Page
1.1 Three key steps in seismic imaging.....	1
1.2 An illustration of the ray paths of seismic events in marine data.....	2
1.3 Typical ray path of primaries in the context of migration techniques as used in this thesis.....	4
1.4 An example of the process of migration.....	7
1.5 An example of the process of migration.....	8
1.6 An example of the process of migration using an incorrect moveout velocity.....	10
2.1 An illustration of a CMP gather before and after NMO correction.....	13
3.1 Typical ray paths of seismic energy in a model comprising two homogeneous half-spaces.....	19
3.2 Effect of Gaussian noise on linear AVA seismic data for different variances of the noise.....	22
3.3 Effect of Gaussian noise on nonlinear AVA seismic data for different variances of the noise.....	23
3.4 Effect of Laplacian noise on linear AVA seismic data for different variances of the noise.....	24
3.5 Effect of Laplacian noise on nonlinear AVA seismic data for different variances of the noise.....	25

FIGURE	Page
3.6 Effect of Rayleigh noise on linear AVA seismic data for different variances of the noise.....	26
3.7 Effect of Rayleigh noise on nonlinear AVA seismic data for different variances of the noise.....	27
3.8 Effect of Uniform noise on linear AVA seismic data for different variances of the noise.....	28
3.9 Effect of Uniform noise on nonlinear AVA seismic data for different variances of the noise.....	29
4.1 AVO Classification based upon reflection coefficient and offset (Barton and Crider, 1999).....	36
4.2 AVO moveout-corrected seismic data of geological model.....	38
4.3 AVO moveout-corrected seismic data used for example 1 and the corresponding statistical averages.....	40
4.4 AVO moveout-corrected seismic data used for example 2 and the corresponding statistical averages.....	41
4.5 AVO moveout-corrected seismic data used for example 3 and the corresponding statistical averages.....	42

CHAPTER I

INTRODUCTION

The three key steps involved in seismic imaging are multiple-attenuation, velocity-analysis, and migration with or without AVO (amplitude variations with offsets), depending on exploration and production objectives. The three steps are performed in the order assigned in Figure 1.1, i.e., demultiple and deghosting followed by velocity estimation followed by migration with or without AVO-A. Let us start by reviewing these three steps.

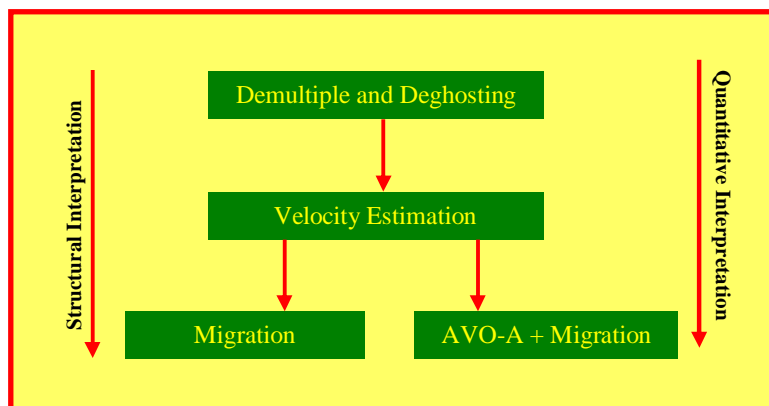


FIGURE 1.1 *Three key steps in seismic imaging. The first steps are demultiple and deghosting and velocity estimation. When followed by migration we obtain the structural image of the subsurface; the interpretation in this case is characterized as structural. When followed by migration with AVO-A we obtain more than the structure of the subsurface. We can also obtain the physical properties of the rock formation; the interpretation in this case is characterized as quantitative.*

This thesis follows the style and format of Geophysics.

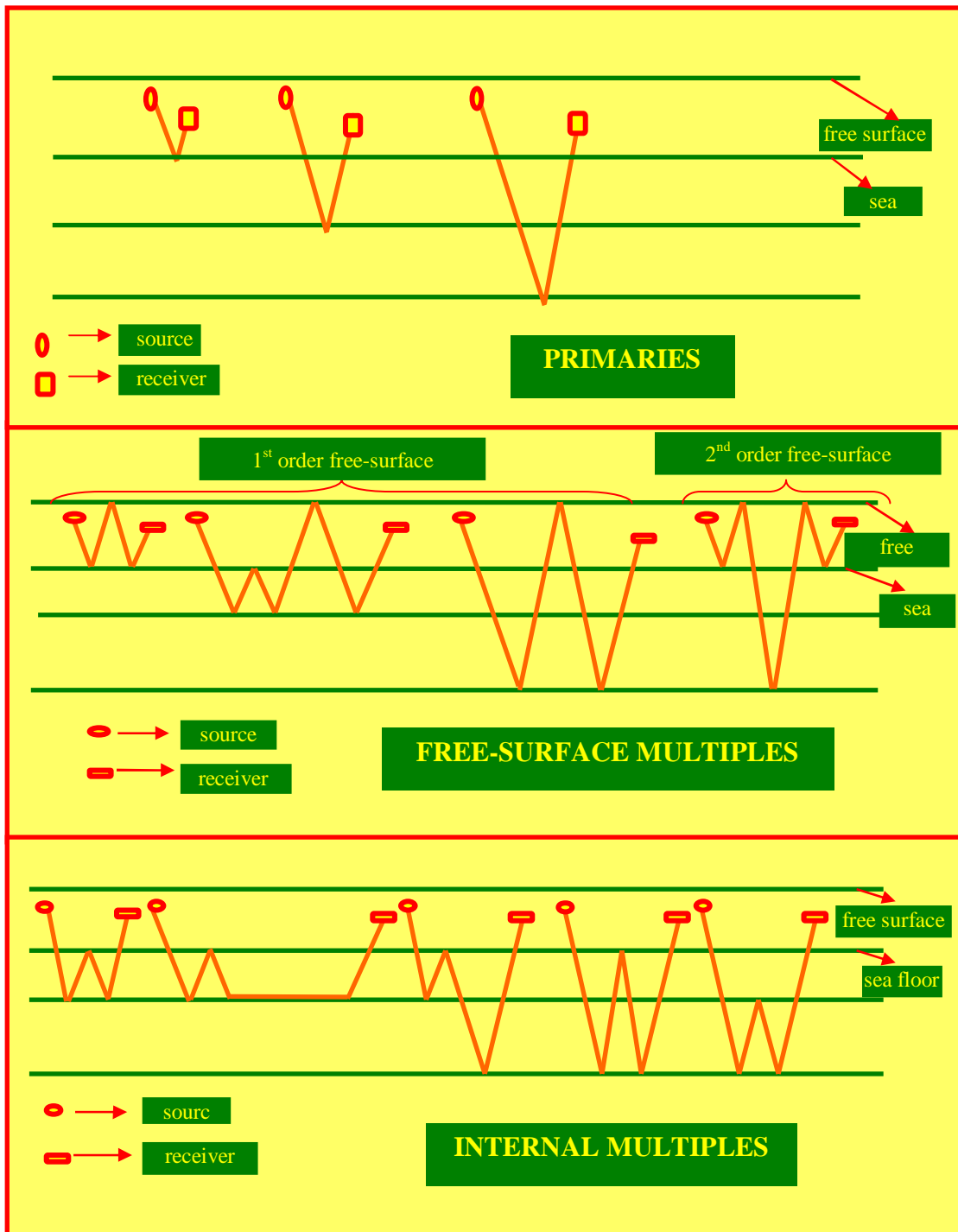


FIGURE 1.2 An illustration of the ray paths of seismic events in marine data.

Seismic data, especially those related to marine acquisition geometries, on which the examples of this thesis are based, contain free-surface multiples, internal multiples and primaries. Figure 1.2 illustrates typical ray paths describing the seismic events in marine data. Note that the common seismic conventions have been used by not taking into account Snell's laws when drawing the ray paths. However, all computations follow Snell's laws.

The goal of the demultiple and deghosting step in seismic imaging is to produce data that are void of multiples and ghosts. In the last two decades, significant efforts have been made to address the multiple-attenuation problem. For example, Watts (2005) and Singh (2005) have presented very efficient algorithms for removing free-surface multiples and demonstrated the feasibility of the technologies in very complex geologies. In this thesis, data containing only primaries will be considered. In other words, it has assumed that multiples have been removed from the data.

We will now consider velocity estimation and the migration of seismic data with only primaries. The velocity estimation and migration steps in seismic imaging are intertwined. Although the velocity model must be estimated before performing migration as described in Figure 1.2, the migration algorithm needs to be formulated first because velocity-estimation is based on the same algorithm as migration.

Let us denote \mathbf{x}_s , the source position, \mathbf{x}_r , the receiver position and \mathbf{x} , the image point, as depicted in Figure 1.3.

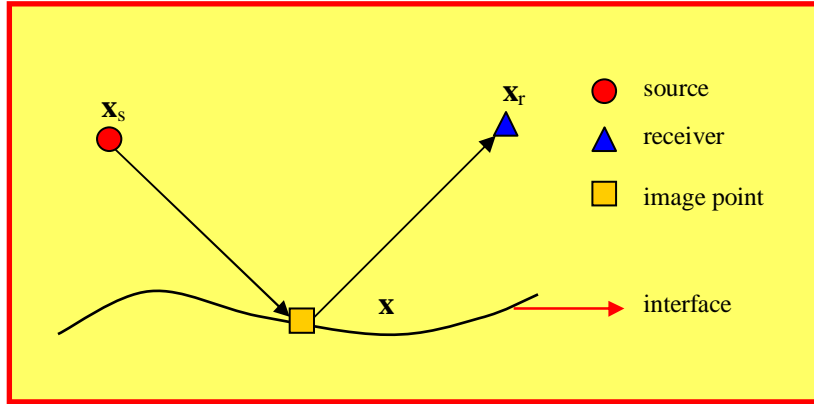


FIGURE 1.3 Typical ray path of primaries in the context of migration techniques as used in this thesis.

A field of primaries can be described in the frequency-space (F-X) domain, as follows:

$$P(\mathbf{x}_s, \mathbf{x}_r, \omega) = \int G(\mathbf{x}_s, \mathbf{x}, \omega) M(\mathbf{x}) G(\mathbf{x}, \mathbf{x}_r, \omega) d\mathbf{x}, \quad (1.1)$$

where $P(\mathbf{x}_s, \mathbf{x}_r, \omega)$ is the field of primaries, $G(\mathbf{x}_s, \mathbf{x}, \omega)$ is the Green's function which describes wave propagation from source to image point, $G(\mathbf{x}, \mathbf{x}_r, \omega)$ is the Green's function which describes wave propagation from image point to receiver, and $M(\mathbf{x})$ characterizes the physical properties of the subsurface. It must be emphasized here that the model used in equation (1.1) to describe our data is only valid for primaries, and hence the assumption that multiples (free-surface multiples and internal multiples) have been attenuated is needed.

Equation (1.1) can also be written as follows:

$$P(\mathbf{x}_s, \mathbf{x}_r, \omega) = \int L(\mathbf{x}_s, \mathbf{x}, \mathbf{x}_r, \omega) M(\mathbf{x}) d\mathbf{x}, \quad (1.2)$$

where $L(\mathbf{x}_s, \mathbf{x}, \mathbf{x}_r, \omega) = G(\mathbf{x}_s, \mathbf{x}, \omega) G(\mathbf{x}, \mathbf{x}_r, \omega)$. The operator L is generally known as the migration operator. One can seek to solve for $M(\mathbf{x})$ through a classical inverse-problem technique such as the least-square-optimization technique. However, if we assume that the data have been corrected for geometrical spreading, the inverse solutions of equation (1.2) can be expressed as follows (Ikelle and Amusden, 2005):

$$M(\mathbf{x}) \approx \int d\mathbf{x}_s \int d\mathbf{x}_r \int d\omega L^*(\mathbf{x}_s, \mathbf{x}, \mathbf{x}_r, \omega) P(\mathbf{x}_s, \mathbf{x}_r, \omega), \quad (1.3)$$

where L^* is the complex conjugate of L . The approximate solution $M(\mathbf{x})$ is known as migration. Notice that the solution in equation (1.3) can be rewritten as follows:

$$M(\mathbf{x}) = \int d\mathbf{x}_s \int d\mathbf{x}_r M'(\mathbf{x}_s, \mathbf{x}, \mathbf{x}_r), \quad (1.4)$$

where $M'(\mathbf{x}_s, \mathbf{x}, \mathbf{x}_r) = \int d\omega L^*(\mathbf{x}_s, \mathbf{x}, \mathbf{x}_r, \omega) P(\mathbf{x}_s, \mathbf{x}_r, \omega)$. This formula depicts the two critical steps involved in migration. The first step involves the computation of $M'(\mathbf{x}_s, \mathbf{x}, \mathbf{x}_r)$, which corresponds to the moveout correction of data. Notice that this computation is equivalent to taking the crosscorrelation of the migration operator L and the data at zero lag. Therefore the operator L must be very similar to the data to produce effective moveout-corrected data. The second step, which corresponds to reconstructing $M(\mathbf{x})$, is equivalent to summing M' over the source and receiver positions. This is known as stack.

To develop more insight into the migration formula (1.4), let us look at the particular case of a 1D model of the earth. In this case, the data $P(\mathbf{x}_s, \mathbf{x}_r, \omega)$ depends only on offset, i.e.

$$P(\mathbf{x}_s, \mathbf{x}_r, \omega) = P(\mathbf{x}_s - \mathbf{x}_r, 0, \omega) = P_{1D}(\mathbf{x}_s - \mathbf{x}_r, \omega) = P_{1D}(\mathbf{x}_h, \omega) \quad (1.5)$$

where $\mathbf{x}_h = \mathbf{x}_s - \mathbf{x}_r$ is the offset and $P_{1D}(\mathbf{x}_h, \omega)$ describes a CMP (common midpoint) gather. In this case, the migration operator L without geometrical spreading becomes (Ikelle and Amusden, 2005):

$$L(\mathbf{x}_h, \omega, z) = \exp \left\{ -i \frac{\omega}{V} \sqrt{\mathbf{x}_h^2 + z^2} \right\} \quad (1.6)$$

To simplify the discussion we have assumed in equation (1.5) that the background velocity is constant and denoted V . Using equation (1.5), the migration in equation (1.4) reduces to:

$$M_{1D}(z) = \int d\mathbf{x}_h M_{1D}'(\mathbf{x}_h, z), \quad (1.7)$$

where $M_{1D}'(\mathbf{x}_h, z) = \int d\omega \exp \left\{ -i \frac{\omega}{V} \sqrt{\mathbf{x}_h^2 + z^2} \right\} d(\mathbf{x}_h, \omega)$.

Figures 1.4 and 1.5 illustrate the various operators introduced in the previous paragraph and the operations associated with them. Four (4) homogeneous half-spaces with a horizontally flat interface have been used to generate the data. The migration operator was then computed using the velocity of the top interface. There must be a similarity between the moveout of the seismic events in our data and that of the

Example 1

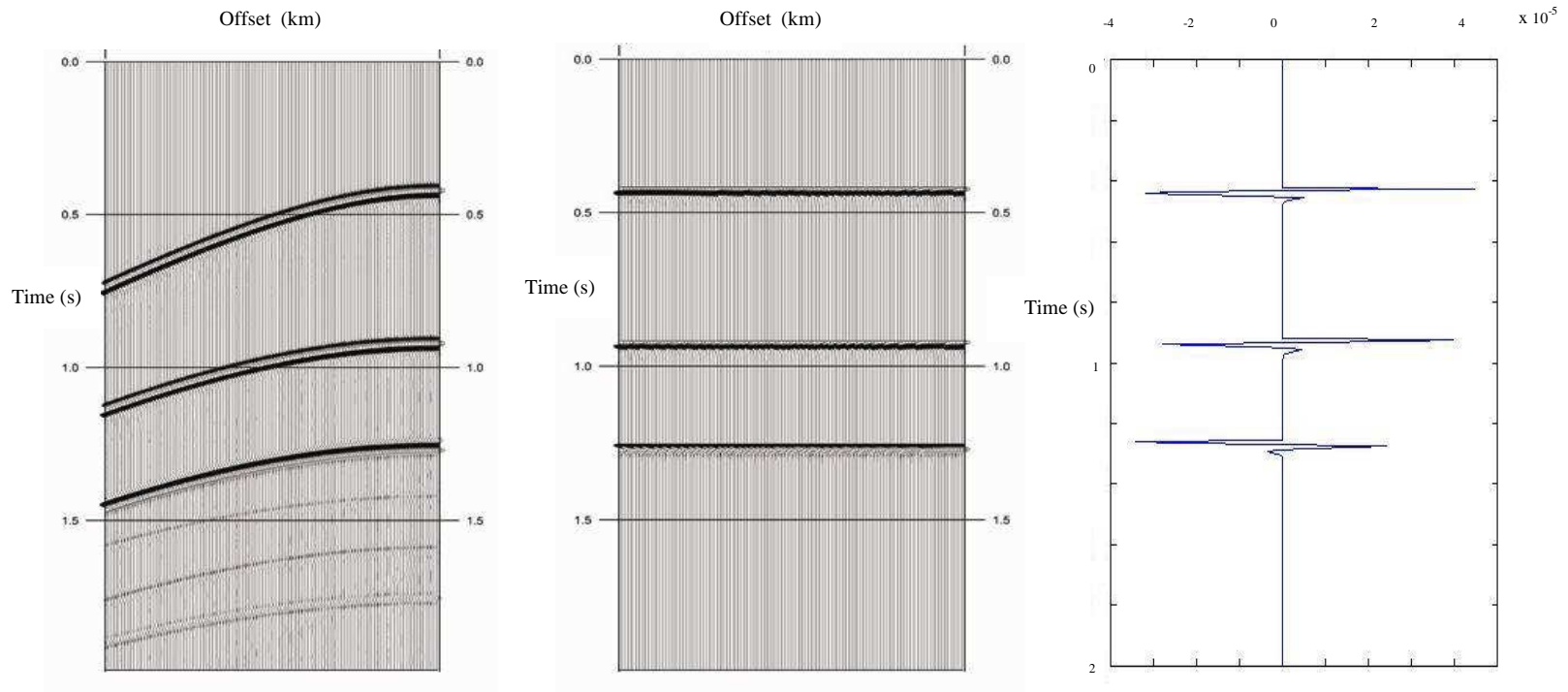


FIGURE 1.4 An example of the process of migration. (a) CMP gather, P_{ID} . (b) Moveout-corrected gather, M_{ID}' , produced using the appropriate moveout velocity. (c) Stack of moveout-corrected data, M_{ID} .

Example 2

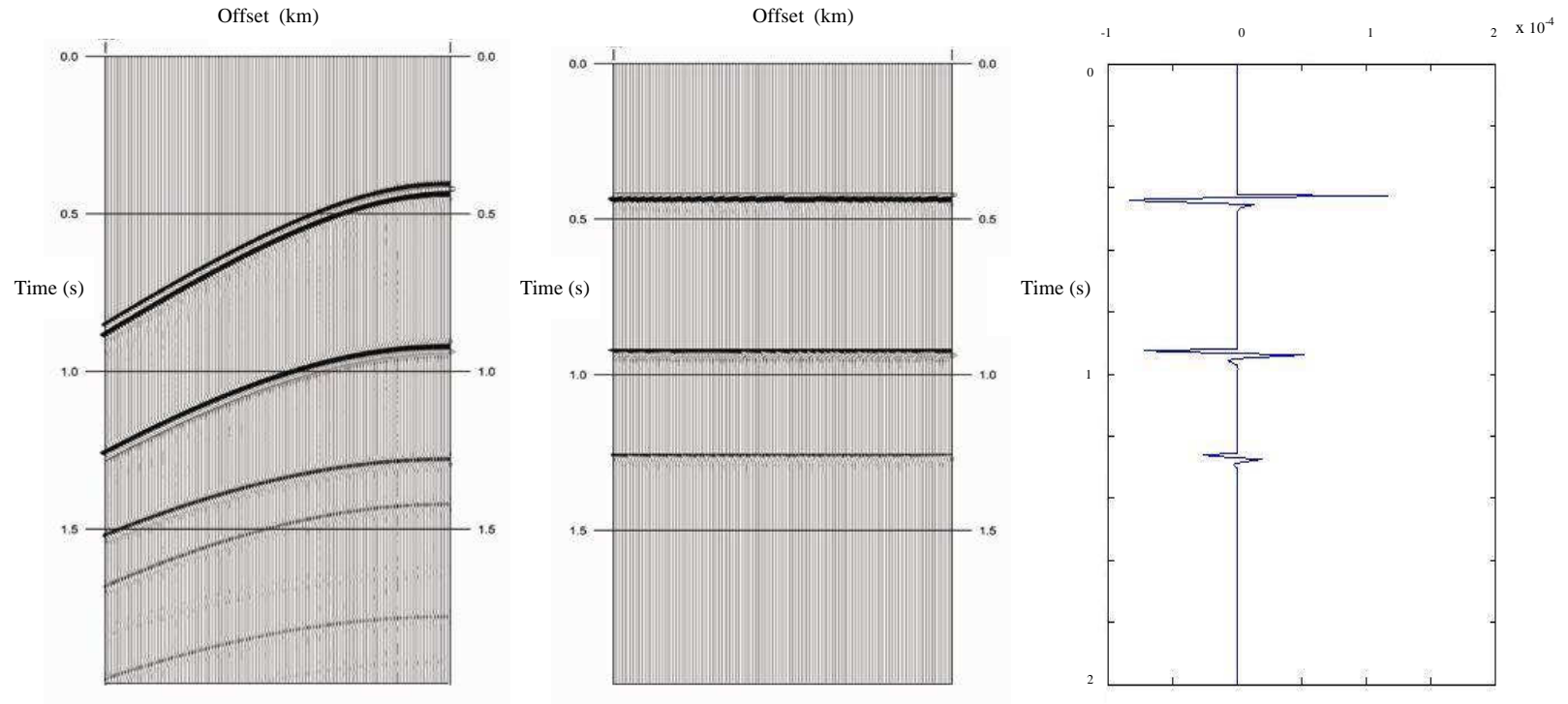


FIGURE 1.5 An example of the process of migration. (a) CMP gather, P_{1D} . (b) Moveout-corrected gather, M_{1D}' , produced using the appropriate moveout velocity. (c) Stack of moveout-corrected data, M_{1D} .

migration operator. The moveout-corrected data, $M_{1D}'(\mathbf{x}_h, z)$, which corresponds to the crosscorrelation of $L(\mathbf{x}_h, \omega, \mathbf{x})$ and $P_{1D}(\mathbf{x}_h, \omega)$ at zero lag, is obviously flat as can be seen in Figures 1.4 and 1.5. Normally, the AVO analysis, which will be discussed later, is taking place on the moveout-corrected data, $M_{1D}'(\mathbf{x}_h, z)$ in Figures 1.4 (c) and 1.5 (c), with each offset converted into reflection angle. The migration is then performed to obtain $M_{1D}(z)$ which allows us to locate the reflector.

Now that we have introduced the migration techniques, let us describe the second step of the processing chain, as depicted in Figure 1.1, i.e. velocity-analysis. As can be seen from the examples in Figures 1.4 and 1.5, the moveout-corrected data is very sensitive to the shape of the migration operator, which in turn is very sensitive to the velocity model. In Figure 1.6 the moveout-corrected migration operator is different from that of the moveout-corrected data. Therefore, $M_{1D}'(\mathbf{x}_h, z)$ in this case is no longer flat. So the basic idea of velocity-analysis consists of computing $M_{1D}'(\mathbf{x}_h, z)$ for various velocity models and selecting the one for which the moveout-corrected data are flat. In this thesis, we will assume that the velocity-analysis has been performed and therefore we assume that we have a correct velocity model.

Assuming that we now have a correct velocity model, $M'(\mathbf{x}_s, \mathbf{x}, \mathbf{x}_r)$ can now be constructed, and from $M'(\mathbf{x}_s, \mathbf{x}, \mathbf{x}_r)$ migrated sections $M(\mathbf{x})$ can be produced, as described in equation (1.3). However, such an image will provide the locations of key reflectors in the subsurface without providing any information about the change of properties that cause the reflections. An alternative approach is to use the moveout-corrected data,

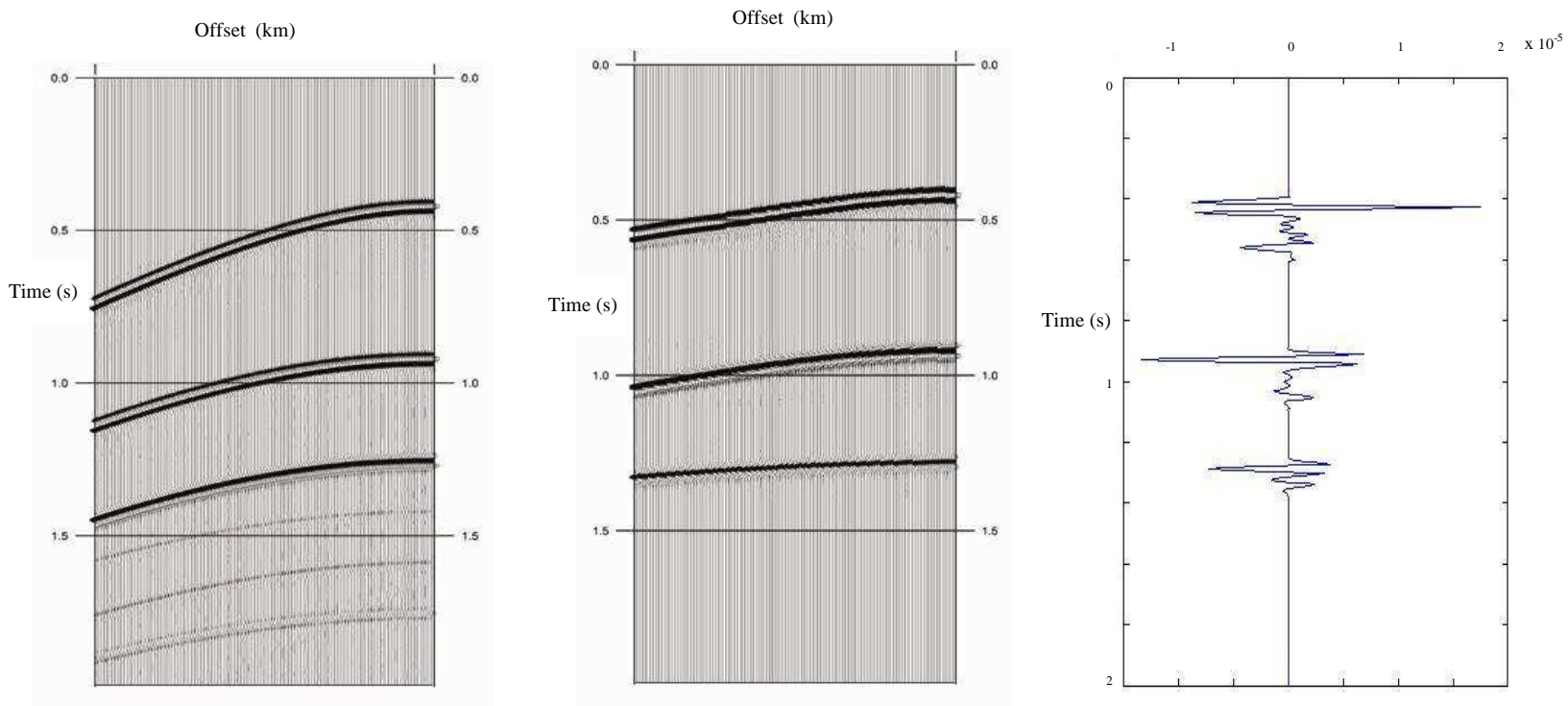


FIGURE 1.6 An example of process of migration using an incorrect moveout velocity. (a) CMP gather, P_{ID} . (b) Moveout-corrected gather, M_{ID}' , produced using an inappropriate moveout velocity. (c) Stack of moveout- corrected data, M_{ID} .

$M'(\mathbf{x}_s, \mathbf{x}, \mathbf{x}_r)$, before stack to characterize the various reflectors. As pointed out earlier, the moveout-corrected data describes how the responses of the seismic data at a specific reflector vary with offsets. If the offsets are converted into angles, it is discovered that the variation of seismic responses with angles (via offsets conversion to angles) is actually a variation of the reflection coefficients with angles.

One of the difficulties of converting offsets into angles is that at each timestep the moveout-corrected response must be converted to AVA (amplitude variations with angles) response. The difficulties of this process arise because the velocity profile that emerges from velocity-analysis is usually smooth. Such a profile may be accurate enough to predict the traveltimes that are needed for constructing the migration operator but are not often good enough to predict the ray bending associated with Snell's law that is needed for converting offsets to reflection angles.

In summary, characterizing reflectors using seismic amplitude variations with offsets is known as AVO analysis. The first step in this process consists of correcting the data for geometrical spreading. In the second step the velocity model is used to produce moveout-corrected data and in the third step the AVO of moveout-corrected data is converted into AVA. And in the final step, the classical small-angle approximation of the reflection coefficient is used, i.e.

$$R_{pp}(\mathbf{x}) = A(\mathbf{x}) + B(\mathbf{x}) \sin^2\theta, \quad (1.8)$$

to recover changes in impedance (which is related to $A(\mathbf{x})$) and Poisson's ratio (which is related to $B(\mathbf{x})$), that are associated with each reflector.

The stack of moveout-corrected data, i.e., $M(\mathbf{x}_s, \mathbf{x}, \mathbf{x}_r)$ in equation (1.4) and $M_{1D}(\mathbf{x}_h, z)$ in equation (1.7), is actually equivalent to taking the mean of these data at each timestep. In this thesis, we propose to compute the variance of the same moveout-corrected data at each timestep. It turns out that outputting both the mean and variance is equivalent to recovering the AVO parameters, $A(\mathbf{x})$ and $B(\mathbf{x})$, without the complex step of converting AVO to AVA. Moreover, the computation of mean and variance can be done in parallel, hence eliminating most of the operations described above. As such, the cost of seismic processing will be significantly reduced, as well as its accuracy, because errors associated with converting offsets to angles will be avoided.

Because seismic events are non-Gaussian, as will be seen in Chapter II, we can also output other cumulants such as skewness and kurtosis. In Chapter II, these cumulants will be described, in addition to recalling the notion of non-Gaussianity and the statistical concepts associated with it. We will demonstrate that outputting these additional cumulants will allow us to characterize rock formations beyond the small-angle approximation. In other words, we are also able to include nonlinear AVO. In Chapter III, preliminary results will be provided that confirm the potential usefulness of these new parameters for characterizing interfaces by discussing one dimensional (1-D) examples.

CHAPTER II

**SOME BACKGROUND OF STATISTICAL AVERAGES OF NON-GAUSSIAN
RANDOM VARIABLES**

Introduction

Let us consider migrated data without stack. Each image/reflection point is illuminated several times as illustrated in Fig 2.1 for 1D medium, as adapted from Ikelle and Amundsen (2005).

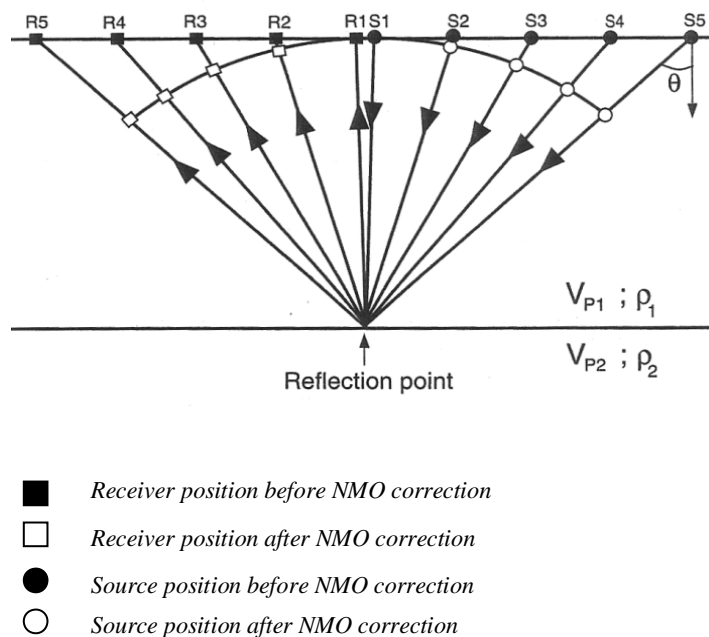


FIGURE 2.1 An illustration of a CMP gather before and after NMO correction. The angle θ is the incident angle.

The image point being imaged consists of N traces that correspond to N source-receiver pairs or offsets. These traces are known as a common midpoint (CMP) gather. If an NMO or travelt ime correction is performed then for all offsets the travelt ime from

source to image point will be identical to the traveltime from image point to receiver. Each offset can now be considered as descriptive of a random event and the set of events as a random variable. Therefore, for each timestep, we can compute the statistical averages.

The classical approach consists of summing the data to produce an image of that point. However, since it is well recognized that the various illuminations contain more information than the classical stack, geophysicists have developed several tools of attribute analysis in order to extract this information. In this thesis, I propose an alternative way of capturing this information. This new statistically based approach consists of treating migrated data without stack as random variables. Hence, the migrated data can be characterized at a given image point by either the statistical moments or cumulants. In Chapters III and IV we will show the applications of this concept.

This chapter focuses on a review of statistical averages, including the averages associated with non-Gaussian random variables, and also on other basic statistical notions that will be needed later on in this analysis.

Moments and Cumulants

Let us denote $M(X, \theta)$ as a random variable at point X . This random variable varies with θ , the reflection angle. The statistical moments of this random variable can be defined as follows:

$$m_n(X, \theta) = E[M^n] = \int_{-\infty}^{\infty} x^n p(x) dx \quad (2.1)$$

where E is the mathematical expectation. For the particular case of the discrete random variable, this can now be defined as:

$$m_n(X, \theta) = \int_{-\infty}^{\infty} x_n^k p(x) dx \quad (2.2)$$

When $n=1$ we have the 1st order moment known as the mean, when $n=2$ we have the 2nd order moment, etc. The migration defined so far in industry corresponds to the 1st order moment (mean) only, and ignores the higher order statistics of the seismic data. Therefore, if we stop here we would lose all the information about the other moments, especially those related to non-Gaussianity.

An alternative way to describe non-Gaussian random variables is to introduce the cumulant. The first four orders are defined in the Table 2.1 below.

TABLE 2.1 *First four orders of cumulants.*

n	Order	Cumulants (c_n)	Statistical Name
1	1 st	c_1	Mean
2	2 nd	c_2	Variance
3	3 rd	c_3	Skewness
4	4 th	c_4	Kurtosis

Using X as a random variable, the relation between cumulants and moments has been described in Table 2.2 below, as adapted from Ikelle and Amundsen (2005). The quantity c_1 (or m_1) is the mean, c_2 (or μ_2) is the variance, c_3 is the skewness and c_4 is the kurtosis.

TABLE 2.2 Relation between the first five moments and cumulants.

n	Moments (m_n)	Central Moments (μ_n)	Cumulants (c_n)	Cumulants (c_n) for zero mean random variable
0	$m_0 = 1$	$\mu_0 = 1$	$c_0 = 0$	$c_0 = 0$
1	$m_1 = E(x)$	$\mu_1 = 0$	$c_1 = m_1$	$c_1 = 0$
2	$m_2 = E(x^2)$	$\mu_2 = m_2 - m_1^2$	$c_2 = m_2 - m_1^2$	$c_2 = m_2$
3	$m_3 = E(x^3)$	$\mu_3 = m_3 - 3 m_2 m_1 + 2 m_1^3$	$c_3 = m_3 - 3 m_2 m_1 + 2 m_1^3$	$c_3 = m_3$
4	$m_4 = E(x^4)$	$\mu_4 = m_4 - 4 m_3 m_1 + 6 m_2 m_1^2 - 3 m_1^4$	$c_4 = m_4 - 4 m_3 m_1 - 3 m_2^2 + 12 m_2 m_1^2 - 6 m_1^4$	$c_4 = m_4 - 3 m_2^2$

For more information on random variables, moments and cumulants see Appendix A.

Non-Gaussian Probability Distributions

The first 2 orders of moments and cumulants (i.e. the mean and variance) are characterized as Gaussian or second order statistics (SOS), and moments and cumulants greater than the second order (e.g. skewness and kurtosis) are characterized as higher order statistics (HOS). When the HOS cumulants are zero they are also characterized as Gaussian, however once the cumulants of order greater than two have non-null values they are characterized as non-Gaussian.

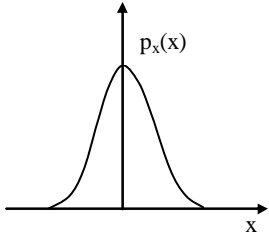
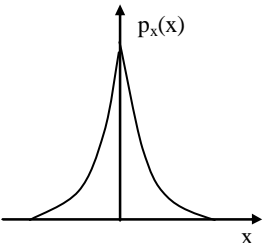
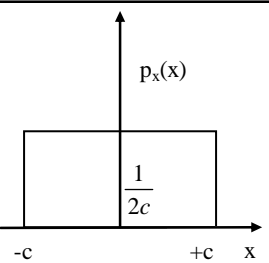
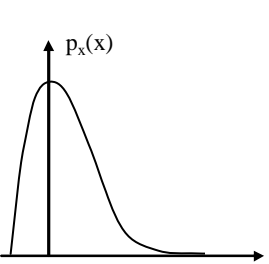
Table 2.3 provides detailed descriptions about the moments and cumulants for different probability density functions. It effectively confirms that for non-Gaussian random variables, the higher order cumulants are non-zero. Notice also that for symmetric distributions the odd cumulants, e.g. the 3rd order cumulant (skewness), are zero. This can clearly be observed with the Laplace and Uniform distributions, chosen because they describe the extreme cases; the Uniform distribution with negative kurtosis (sub Gaussian) and the Laplace distribution with positive kurtosis (super Gaussian).

In Table 2.3, the Rayleigh distribution shows an example of non-Gaussian, non-symmetric random variables. We can see that when the random variable is non-Gaussian and non-symmetric that we have extra information through both the skewness and kurtosis.

To date, the extra information that can be captured in the HOS has not yet been exploited in seismic data processing. Practical seismic data processing is actually limited to the mean, since the variance is not really used. Techniques based on SOS recover only limited information about non-Gaussian signals, and as such information related to deviations from Gaussianity is not extracted. Better results can be realized using HOS over SOS, since HOS allows for the processing of seismic signals that are non-Gaussian. Studying the higher order statistics will allow information extra to that used in traditional seismic imaging to be utilized. This will enable better estimates of parameters in noisy situations or shed light on non-linearities that may be inherent in the seismic data.

One of challenges that will be addressed in the next chapter is not only recovery of the seismic attributes: the mean, variance, skewness and kurtosis for each image point, but also connecting this new information to specific geologies. For example, in areas where the reflection coefficient can be described by $R = A + B x$, the skewness and kurtosis are expected to be zero. Here A will basically characterize the mean and B can characterize the variance. In other words, the statistical averages can be used to recover A or B at small angles. As more realistic cases are considered, HOS can then be utilized to characterize the other parameters.

TABLE 2.3 First four moments and cumulants of the Gaussian, Laplace, Uniform and Rayleigh distributions.

Gaussian Distribution			
	$p_x(x) = \frac{1}{\sqrt{2\pi}\sigma} \exp(-x^2/2\sigma^2)$		
	n	$m_x^{(n)}$	$c_x^{(n)}$
	1	0	0
	2	σ^2	σ^2
	3	0	0
	4	$3\sigma^4$	0
Laplace Distribution			
	$p_x(x) = \frac{\lambda}{2} \exp(-\lambda x)$		
	n	$m_x^{(n)}$	$c_x^{(n)}$
	1	0	0
	2	$2/\lambda^2$	$2/\lambda^2$
	3	0	0
	4	$24/\lambda^4$	$12/\lambda^4$
Uniform Distribution			
	$p_x(x) = \frac{1}{2c} \quad x \in [-c, +c]$		
	n	$m_x^{(n)}$	$c_x^{(n)}$
	1	0	0
	2	$c^2/3$	$c^2/3$
	3	0	0
	4	$3c^4/5$	$-2c^4/15$
Rayleigh Distribution			
	$p_x(x) = x/\alpha^2 \exp(-x^2/2\alpha^2) \quad x \geq 0$		
	n	$m_x^{(n)}$	$c_x^{(n)}$
	1	$\alpha \sqrt{\frac{\pi}{2}}$	$\alpha \sqrt{\frac{\pi}{2}}$
	2	$2\alpha^2$	$(2 - \frac{\pi}{2}) \alpha^2$
	3	$3\alpha^3 \sqrt{\frac{\pi}{2}}$	$-3\alpha^3 (1 - \frac{\pi}{3}) \sqrt{\frac{\pi}{2}}$
	4	$8\alpha^4$	$1/2\alpha^4 (12\pi - 3\pi^2 - 8)$

CHAPTER III

HOS AND AVO SEISMIC DATA

Introduction

Energy is partitioned into reflected and transmitted energy at an interface that separates two different layers, as illustrated in Figure 3.1. The reflection and transmission is dependent on the angle of incidence, θ of the incoming wave, as well as the physical properties of the two layers. The seismic amplitudes of the reflected and transmitted energy depend on the contrast in the physical properties across the boundary, i.e. the amplitudes carry information about the contrast of elastic parameters of two (2) rock formations. The Zoeppritz equations, which define the reflection and transmission coefficients, are used to relate the reflected and transmitted energy to the physical properties of the two layers. In this thesis, we will only refer to the reflection coefficient.

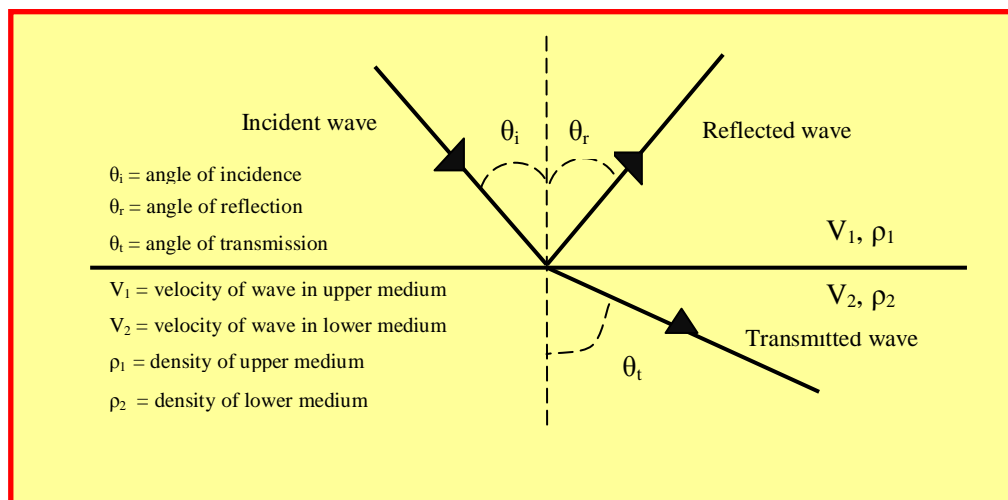


FIGURE 3.1 Typical ray paths of seismic energy in a model comprising two homogeneous half-spaces.

The linearized expressions of the Zoeppritz equations are derived using the small-angle approximation. For the reflection coefficient the linear approximation can be given by:

$$R = A + B x \quad (3.1)$$

where $x = \sin^2\theta$

At larger angles, the reflection coefficient can be given by:

$$R = A + B x + C x^2 \quad (3.2)$$

This is a second order approximation in x . Numerically it has been shown that the linear approximation works best for angles of $\theta < 35^\circ$ and the second order approximation works best for angles of $\theta < 60^\circ$, after which the expressions become unstable.

These approximations produce small inaccuracies and are incorporated in the seismic data as noise. In practice, the noise associated with the seismic data acquisition geometries is also integrated into the data. For this reason, the reflection coefficient given in equation (3.2) above can now be described by:

$$R = A + B x + C x^2 + \eta = R_o + \eta \quad (3.3)$$

where $R_o = A + B x + C x^2$

In this thesis we will describe R_o and η as two (2) random variables.

Examples of the Effect of Noise on CMP AVA Seismic Data

Consider several examples of CMP AVA data in Figures 3.2 to 3.9. These examples show the effect of adding different types and variances of noise to linear and nonlinear AVA. Each figure contains four (4) diagrams of the AVA data and their associated histograms, as the variance of the noise added is increased. We have also computed the corresponding statistical averages for these examples as illustrated in Table 3.1.

Analysis of Results

From the histograms, we can observe that as the order of the noise is increased, the data tends more and more toward the type of noise that is added. It is also clear that seismic data does not tend to the Gaussian distribution. Therefore, we can characterize seismic data at a given image point as non-Gaussian random variables. The experiment was repeated several times giving the same conclusion that the seismic data behaved more like a non-Gaussian distribution.

So one might ask the following question: In what cases can seismic data be described by a Gaussian random variable? One possible case is that the seismic response is invariant with the reflection angle. This is however non physical, since we can see from the Zoeppritz equations that it is impossible to have constant reflection coefficient with angle. Alternatively, we can get a Gaussian distribution if the reflection coefficients

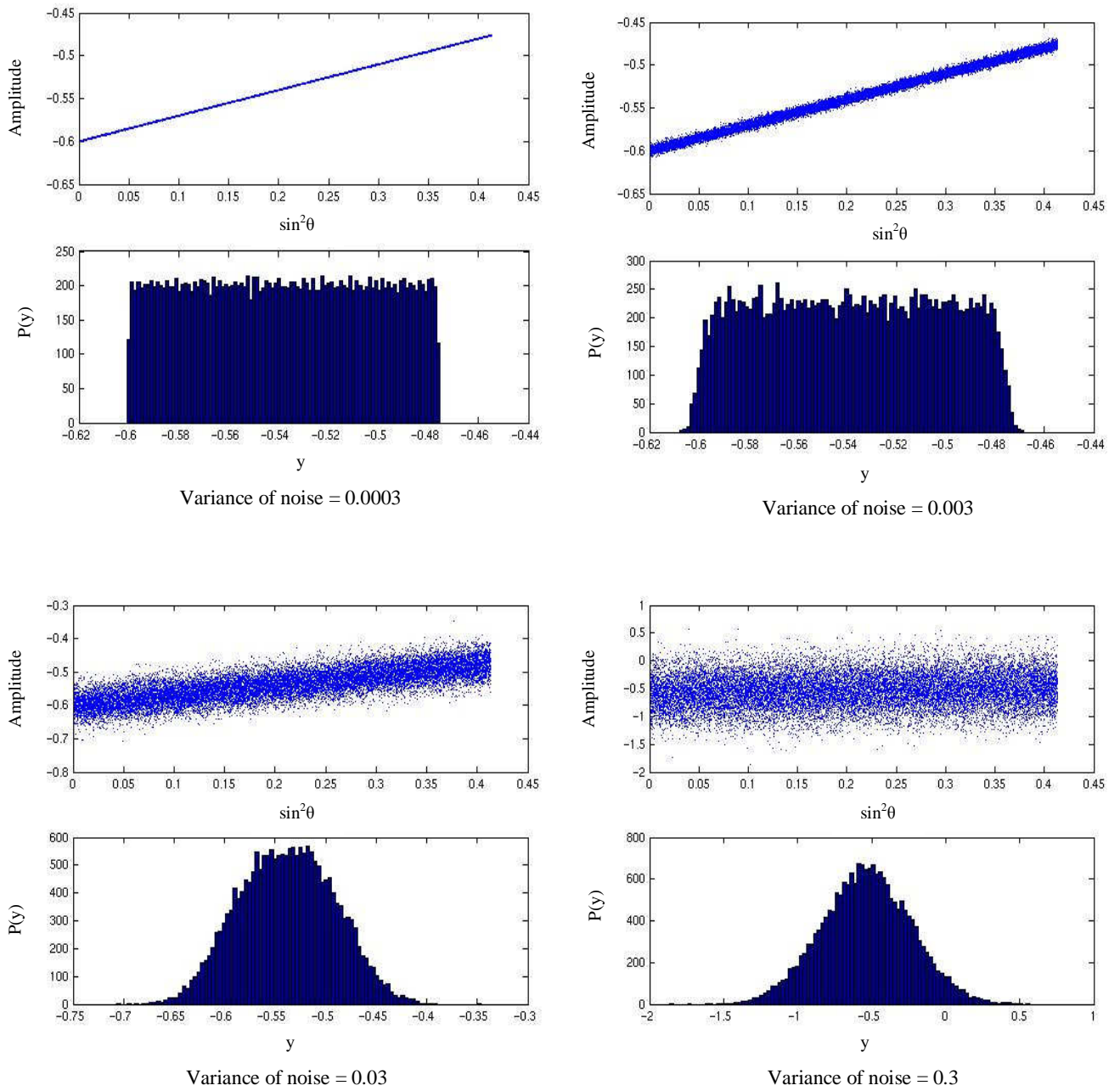


FIGURE 3.2 Effect of Gaussian noise on linear AVA seismic data for different variances of the noise.

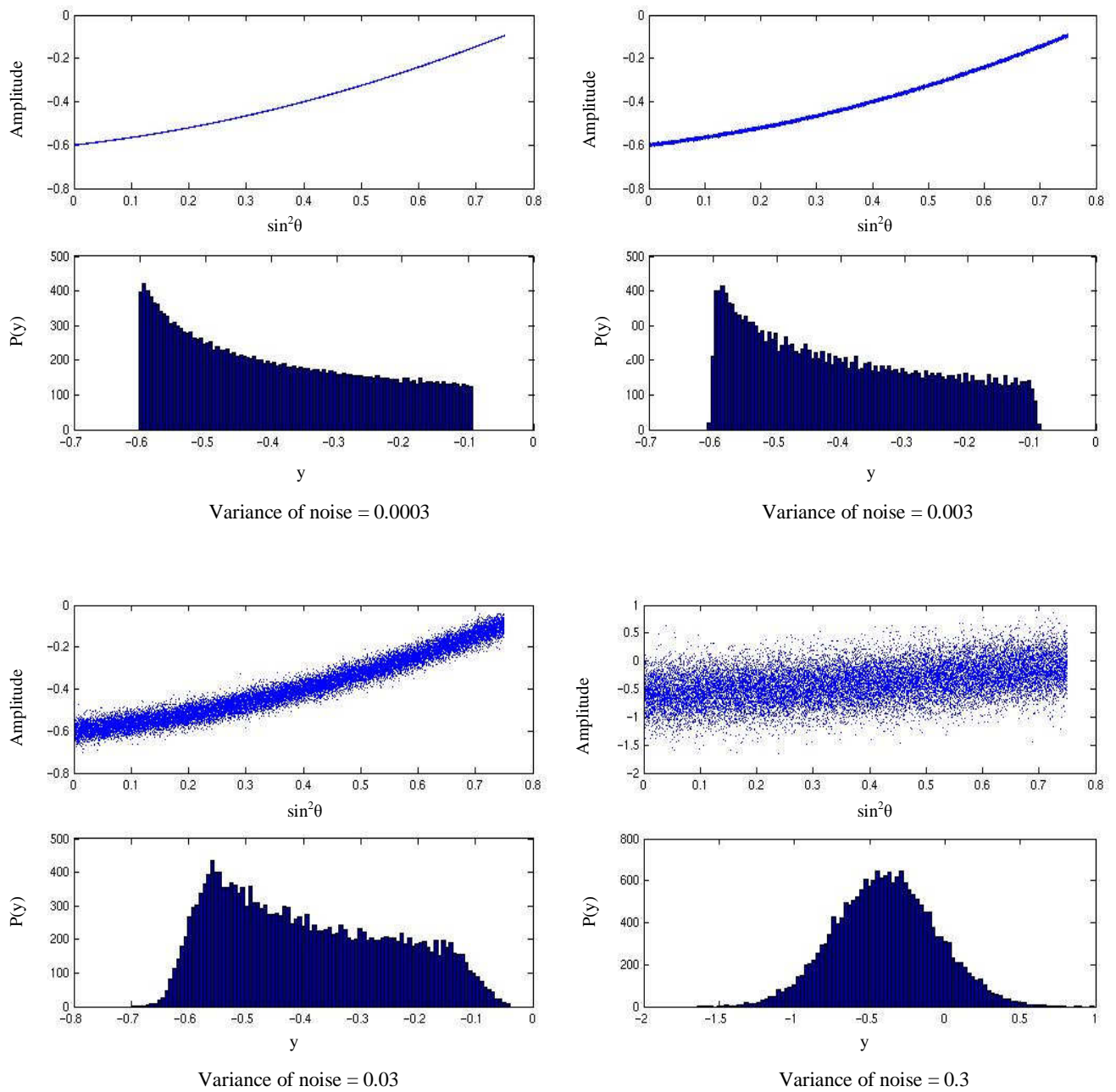


FIGURE 3.3 Effect of Gaussian noise on nonlinear AVA seismic data for different variances of the noise.

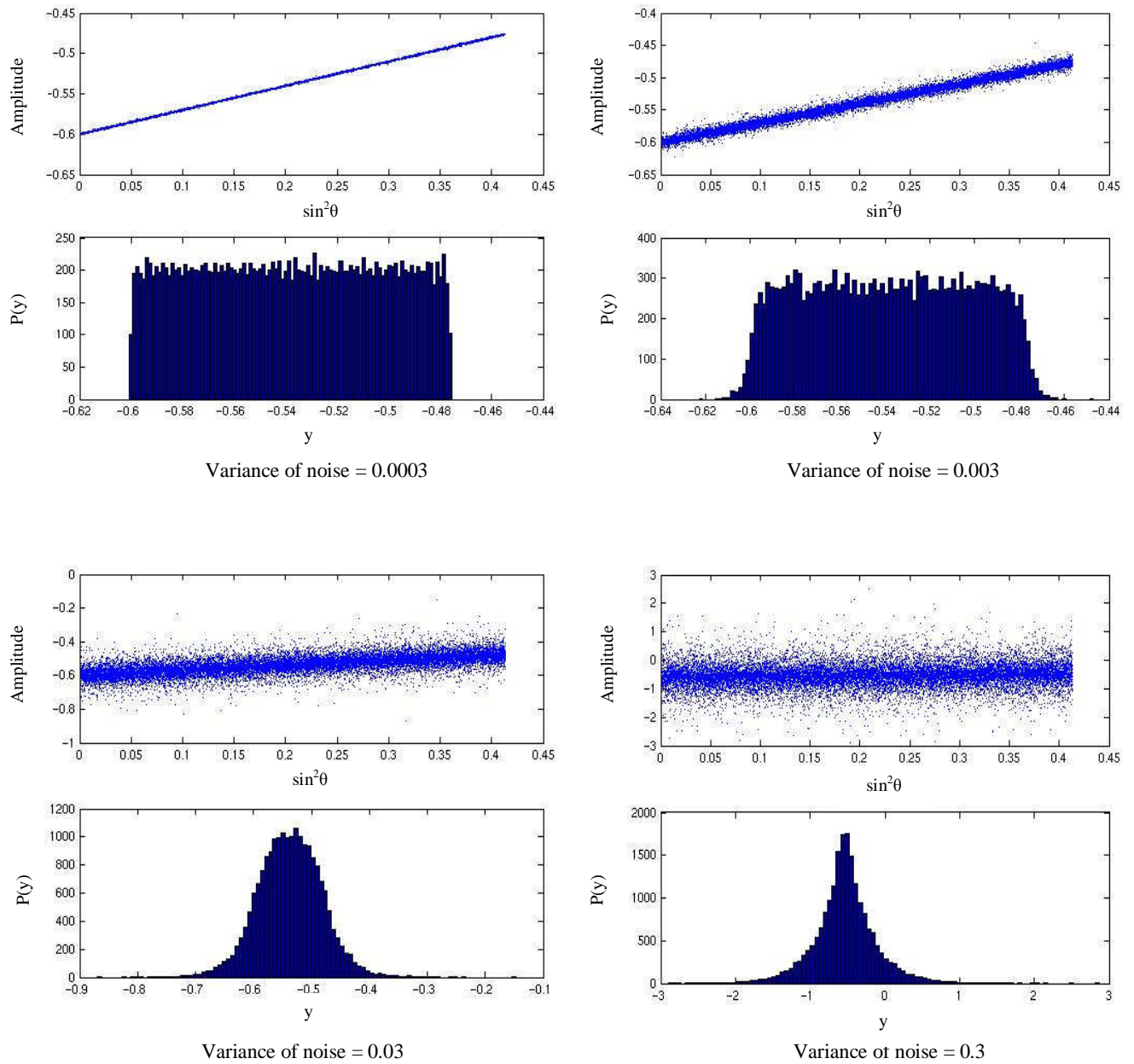


FIGURE 3.4 Effect of Laplacian noise on linear AVA seismic data for different variances of the noise.

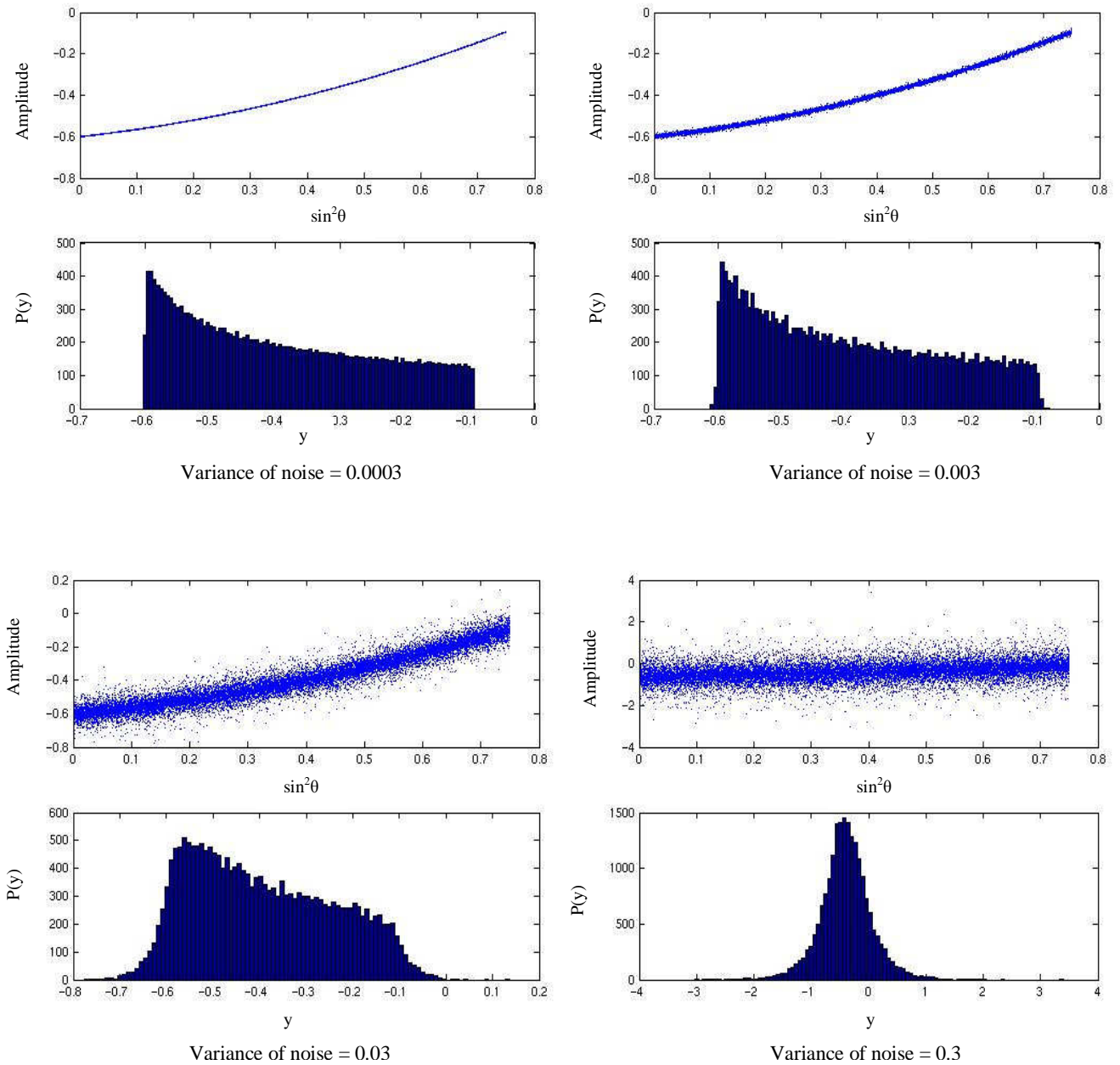


FIGURE 3.5 Effect of Laplacian noise on nonlinear AVA seismic data for different variances of the noise.

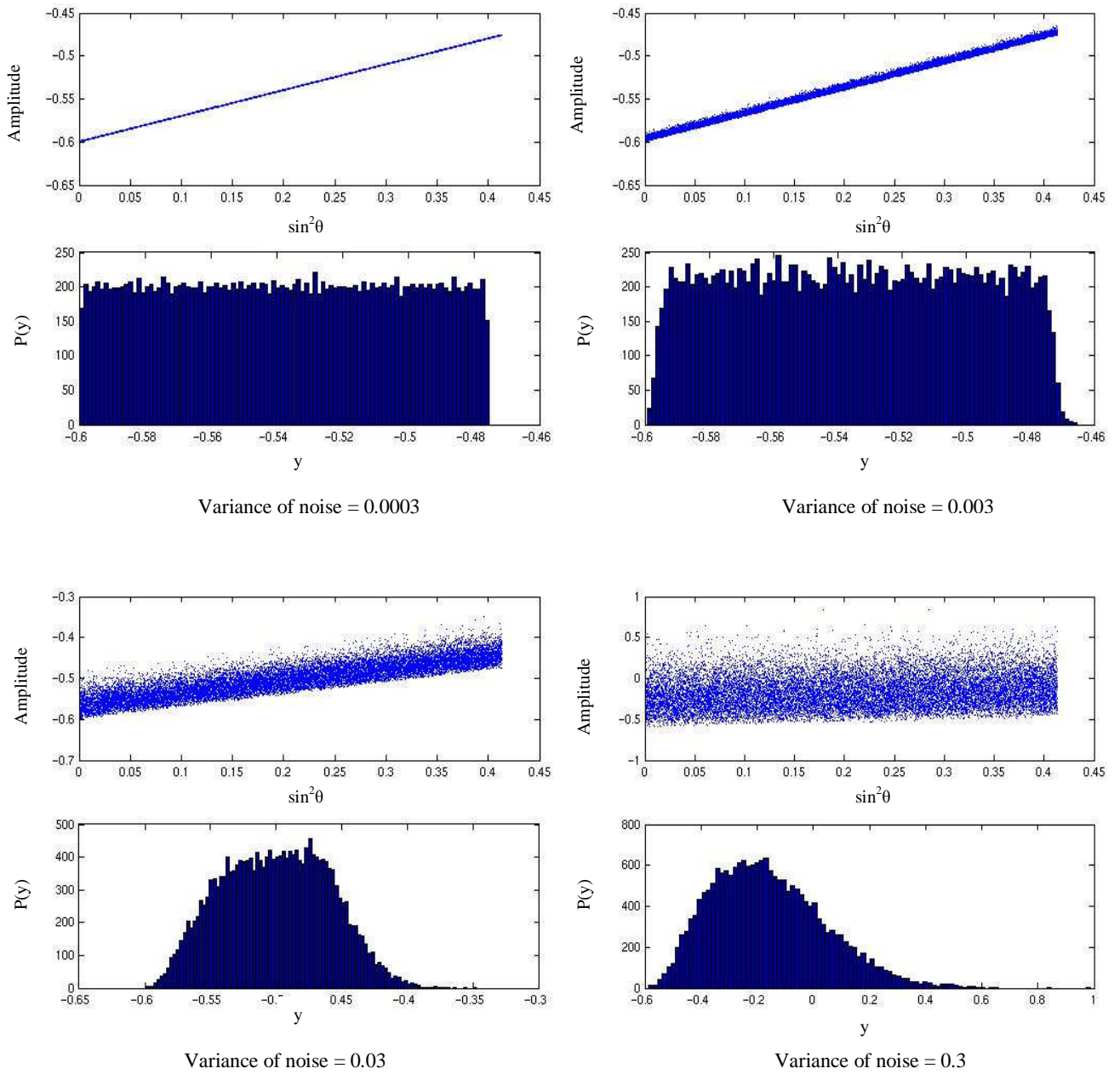


FIGURE 3.6 Effect of Rayleigh noise on linear AVA seismic data for different variances of the noise.

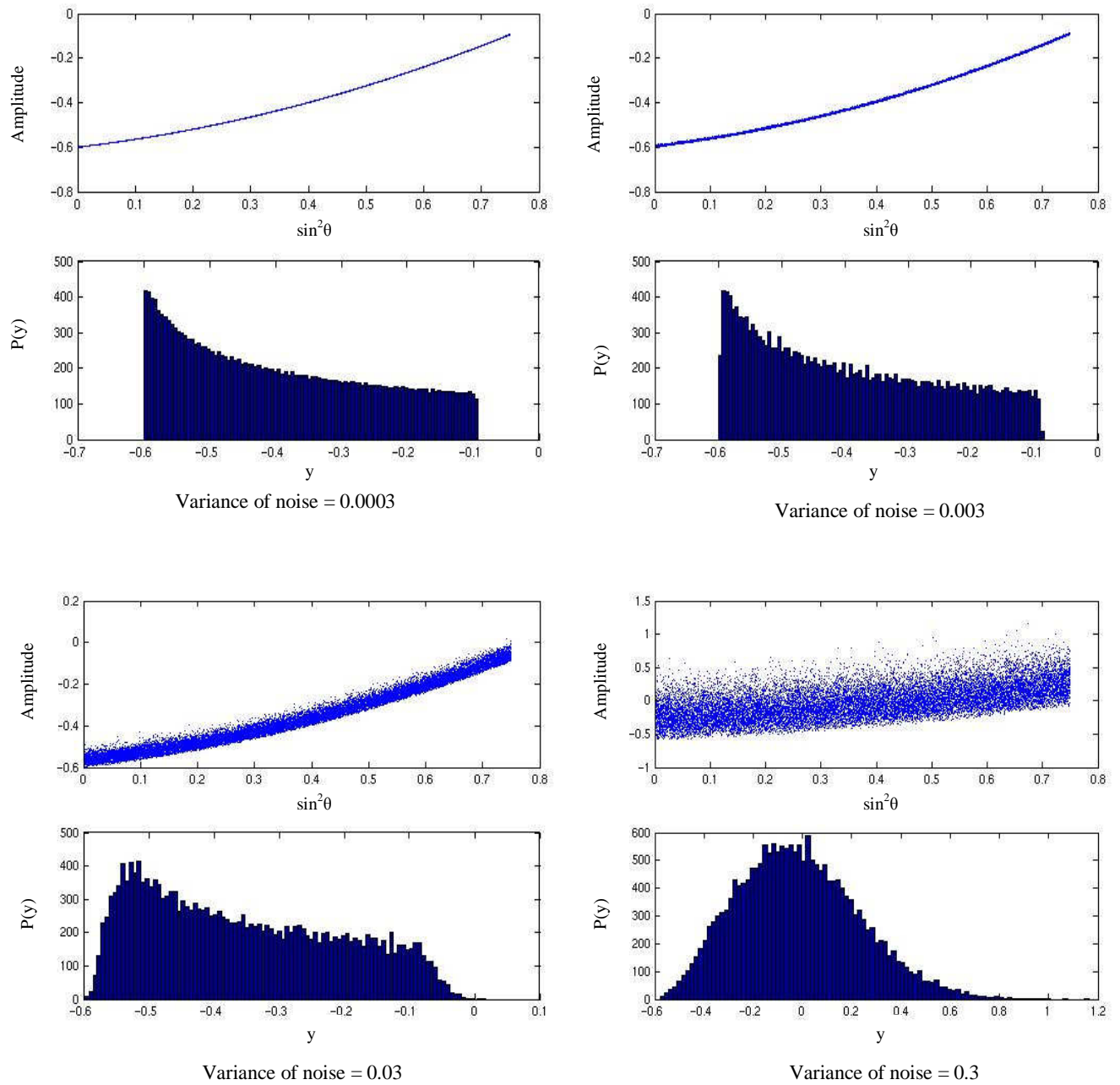


FIGURE 3.7 Effect Rayleigh noise on nonlinear AVA seismic data for different variances of the noise.

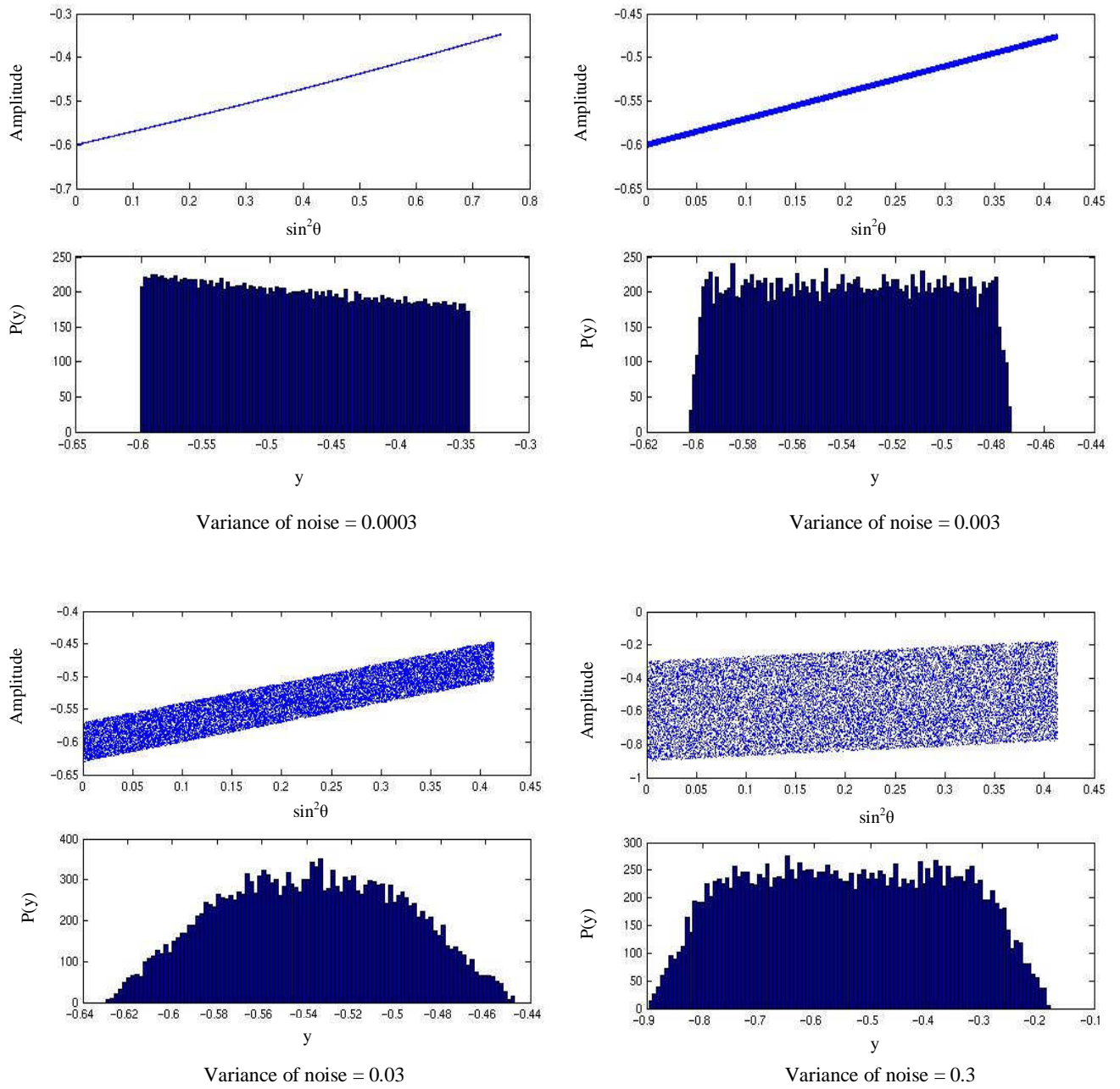


FIGURE 3.8 Effect of Uniform noise on linear AVA seismic data for different variances of the noise.

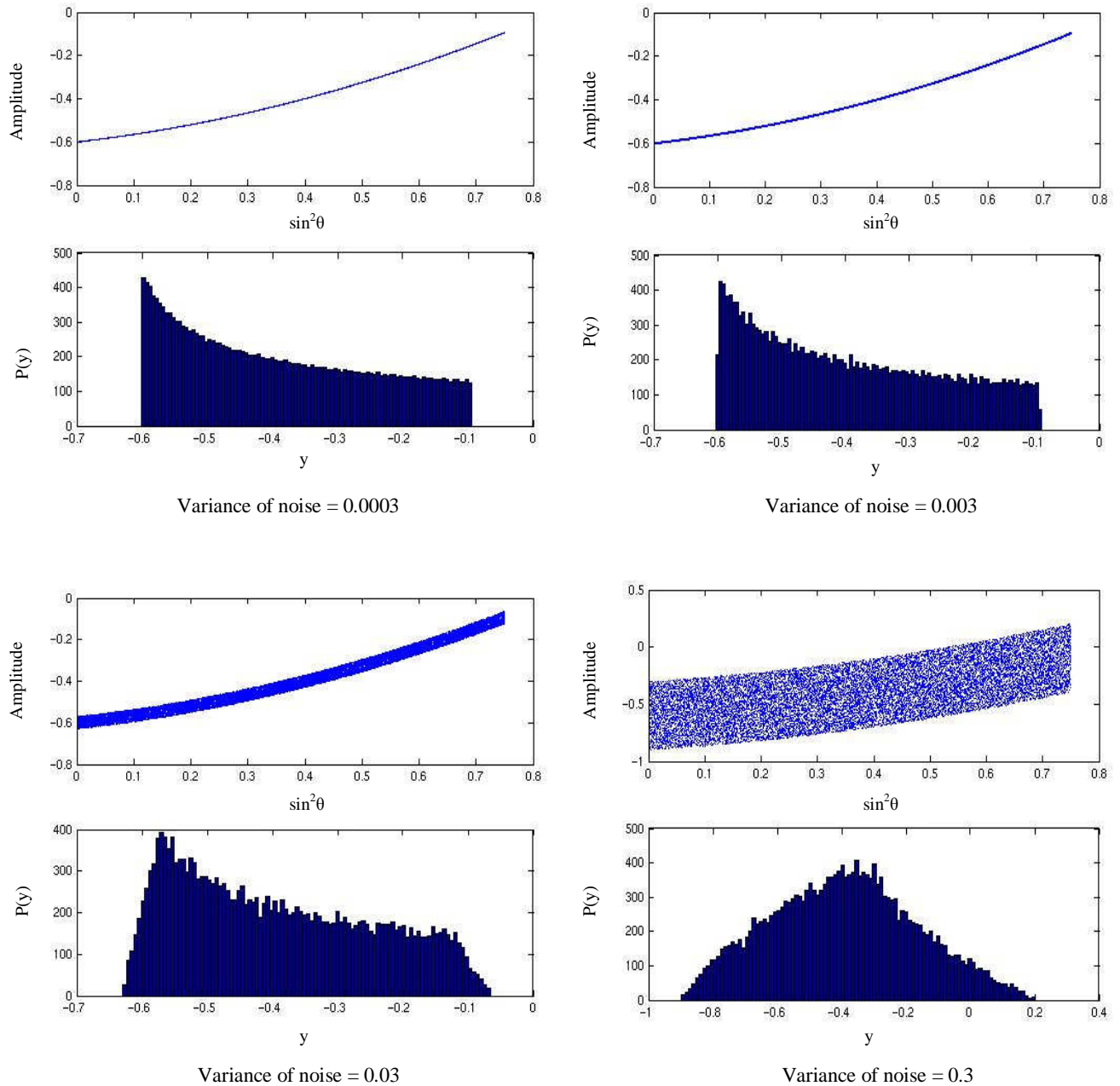


FIGURE 3.9 Effect of Uniform noise on nonlinear AVA seismic data for different variances of the noise.

TABLE 3.1 Statistical averages of AVO seismic data for different types and variances of additive noise presented in Figures 3.2 to 3.9.

Gaussian (Linear)				
Variance of Noise	Mean	Variance	Skewness	Kurtosis
0.0003	-0.538025	0.0012805	0.000172566	-0.0429237
0.003	-0.538022	0.00128765	0.000619463	-0.0424862
0.03	-0.538384	0.00218992	0.00316914	-0.0191433
0.3	-0.538449	0.0901212	0.0134413	0.00424079
Gaussian (Non-linear)				
Variance of Noise	Mean	Variance	Skewness	Kurtosis
0.0003	-0.393761	0.0217956	0.375146	-0.160141
0.003	-0.393801	0.0218062	0.375577	-0.159903
0.03	-0.393533	0.0226981	0.347874	-0.153352
0.3	-0.391978	0.111797	0.0458331	-0.00273106
LaPlacian (Linear)				
Variance of Noise	Mean	Variance	Skewness	Kurtosis
0.0003	-0.538027	0.00128005	1.90102e-05	-0.0429171
0.003	-0.538029	0.00129885	-0.00229077	-0.0420918
0.03	-0.537569	0.00311477	-0.012903	0.0590645
0.3	-0.536581	0.178466	0.0516943	1.27223
LaPlacian (Non-linear)				
Variance of Noise	Mean	Variance	Skewness	Kurtosis
0.0003	-0.393773	0.0217951	0.37518	-0.160133
0.003	-0.393801	0.0218226	0.374189	-0.160052
0.03	-0.393542	0.0235839	0.328764	-0.140445
0.3	-0.394912	0.201337	0.090346	1.09169
Rayleigh (Linear)				
Variance of Noise	Mean	Variance	Skewness	Kurtosis
0.0003	-0.537653	0.0012804	-3.13495e-05	-0.0429372
0.003	-0.534257	0.00128375	0.000470458	-0.0427205
0.03	-0.50051	0.00164901	0.0507358	-0.0277204
0.3	-0.160657	0.0404481	0.588773	0.0420479
Rayleigh (Non-linear)				
Variance of Noise	Mean	Variance	Skewness	Kurtosis
0.0003	-0.393385	0.0217955	0.375145	-0.160138
0.003	-0.389972	0.021791	0.374719	-0.160138
0.03	-0.35611	0.0222127	0.368259	-0.156131
0.3	-0.0173828	0.0605068	0.399546	-0.00997649
Uniform (Linear)				
Variance of Noise	Mean	Variance	Skewness	Kurtosis
0.0003	-0.538026	0.00128048	4.09828e-05	-0.042938
0.003	-0.538055	0.00128321	-0.000890827	-0.0427528
0.03	-0.538072	0.0015817	-0.00317656	-0.0329229
0.3	-0.538883	0.0311004	0.00700946	-0.193539
Uniform (Non-linear)				
Variance of Noise	Mean	Variance	Skewness	Kurtosis
0.0003	-0.393764	0.0217959	0.375178	-0.160142
0.003	-0.393768	0.0217955	0.375155	-0.160066
0.03	-0.393782	0.0220683	0.367511	-0.156631
0.3	-0.393237	0.0508386	0.106608	-0.128628

vary in the form, $R = A + B \sin^2\theta$, where θ are uniformly distributed. Because seismic data are sampled in offset, this scenario is also unrealistic. Thus, the random variables of interest in this analysis are non-Gaussian most of the time.

Let us focus consider the histograms and statistics obtained for each example. In all cases we can see that for very little variance of additive noise, the data is non-Gaussian. The data is Uniform in the linear AVA case. As the variance of the noise is increased to the point where there is too much noise, the data tend to the distribution of the noise added.

For the case of the additive Gaussian noise with the linear AVA data, we see that as the variance of the noise increases, the data tend toward a Gaussian distribution and with the nonlinear AVA, the data tend toward a nonsymmetric non-Gaussian distribution, i.e.

Linear AVO + Gaussian noise \longrightarrow Gaussian data

Nonlinear AVO + Gaussian noise \longrightarrow nonsymmetric, non-Gaussian data

There is a significant increase in the variance, skewness and kurtosis in the nonlinear AVA case when compared to the linear AVA case. Again showing that despite the noise being Gaussian, the data have been rendered non-Gaussian because of the nonlinear AVA effect.

Consider the case of non-Gaussian noise with symmetric distributions, i.e. Laplacian and Uniform noise. For additive Laplacian noise with the linear AVA data, we see that as the variance of the noise increases, the data tend toward a symmetric, super

non-Gaussian distribution and with the nonlinear AVA, the data tend toward a nonsymmetric non-Gaussian distribution, i.e.

Linear AVO + Laplacian noise \longrightarrow symmetric, super non-Gaussian data

Nonlinear AVO + Laplacian noise \longrightarrow nonsymmetric, non-Gaussian data

For additive Uniform noise with the linear AVA data, we see that as the variance of the noise increases, the data tend toward a symmetric, sub non-Gaussian distribution and with the nonlinear AVA, the data tend toward a nonsymmetric non-Gaussian distribution, i.e.

Linear AVO + Uniform noise \longrightarrow symmetric, sub non-Gaussian data

Nonlinear AVO + Uniform noise \longrightarrow nonsymmetric, non-Gaussian data

For both types of additive noise, for the linear AVA case, the skewness is almost null for all variances of noise, whereas in the nonlinear case the skewness is large and generally constant for all variances of noise. The kurtosis in the linear AVA case though smaller is significant and increases slightly, just as in the nonlinear case. For the Laplacian additive noise, the kurtosis tends more to a positive value (super Gaussian), whereas for the Uniform additive noise it tends to a more negative value (sub Gaussian). Hence, in order to distinguish between Gaussian noise and non-Gaussian noise with symmetric distributions, the kurtosis must be examined.

For the case of the non-Gaussian noise with nonsymmetric distributions, i.e. Rayleigh noise, we see that with the both the linear and nonlinear AVA data, as the variance of the noise increases, the data tend toward a nonsymmetric non-Gaussian distribution.

Linear AVO + Rayleigh noise \longrightarrow nonsymmetric, non-Gaussian data

Nonlinear AVO + Rayleigh noise \longrightarrow nonsymmetric, non-Gaussian data

There is a significant increase in the skewness as the variance of the noise increases. Similar to the Laplacian and Uniform noise, the kurtosis in the linear AVA case though smaller is significant and increases slightly, just as in the nonlinear case.

Summarizing, we can say that the skewness can be used to characterize nonsymmetric, non-Gaussian noise and the kurtosis can be used to characterize symmetric, non-Gaussian noise in the data. Non-Gaussian data result from either the presence of non-linear AVA effects or non-Gaussian noise. Also, since seismic data are generally considered to be statistically symmetric, any significant value of skewness may indicate bad processing and in this case it could be that the moveout correction was not performed correctly.

CHAPTER IV

ANALYSIS OF HOS MIGRATION THROUGH ONE-DIMENSIONAL

GEOLOGICAL MODELS

The standard migration algorithm used in conventional seismic migration consists of two major processes, moveout correction and then the stack of the moveout-corrected data; as described earlier in Chapter I. Our formulation of this HOS migration algorithm is based on adapting only the stack component of the standard algorithm. Assuming that the moveout correction has been performed accurately, the stack component is improved such that more information present in the seismic data can be output from the new algorithm.

Formulation of the HOS Migration Algorithm

The formulation of the HOS migration algorithm is based on treating the moveout-corrected data as a random variable, as discussed before. This moveout-corrected data is defined by:

$$M'(\mathbf{x}_s, \mathbf{x}, \mathbf{x}_r) = \int d\omega L^*(\mathbf{x}_s, \mathbf{x}, \mathbf{x}_r, \omega) P(\mathbf{x}_s, \mathbf{x}_r, \omega) \quad (4.1)$$

Traditional migration then sums this data over the receivers and sources to produce the stack.

$$M(\mathbf{x}) = \int d\mathbf{x}_s \int d\mathbf{x}_r M'(\mathbf{x}_s, \mathbf{x}, \mathbf{x}_r) \quad (4.2)$$

where $P(\mathbf{x}_s, \mathbf{x}_r, \omega)$ is the seismic data in the F-X domain and $L(\mathbf{x}_s, \mathbf{x}, \mathbf{x}_r, \omega)$ is the migration operator, as introduced in the previous chapter.

Instead of outputting only the stack, from the moveout-corrected data we can output the parameters $m_1(\mathbf{x})$ to $m_4(\mathbf{x})$ as defined below:

$$m_1(\mathbf{x}) = \int d\mathbf{x}_s \int d\mathbf{x}_r M'(\mathbf{x}_s, \mathbf{x}, \mathbf{x}_r), \quad (4.3)$$

$$m_2(\mathbf{x}) = \int d\mathbf{x}_s \int d\mathbf{x}_r (M'(\mathbf{x}_s, \mathbf{x}, \mathbf{x}_r))^2, \quad (4.4)$$

$$m_3(\mathbf{x}) = \int d\mathbf{x}_s \int d\mathbf{x}_r (M'(\mathbf{x}_s, \mathbf{x}, \mathbf{x}_r))^3, \quad (4.5)$$

$$m_4(\mathbf{x}) = \int d\mathbf{x}_s \int d\mathbf{x}_r (M'(\mathbf{x}_s, \mathbf{x}, \mathbf{x}_r))^4, \quad (4.6)$$

These parameters actually define the statistical moments as described in Table (2.2). The parameter $m_1(\mathbf{x})$ is actually the stack in the standard migration algorithm. Using $m_1(\mathbf{x})$ to $m_4(\mathbf{x})$ the new algorithm can now output the parameters variance, skewness and kurtosis in addition to the mean. These three (3) additional cumulants are defined in Table (4.1) below.

TABLE 4.1 *Output parameters of HOS migration.*

OUTPUT PARAMETERS	EQUATIONS DEFINING THE OUTPUT PARAMETERS
Mean, $M(\mathbf{x})$	$m_1(\mathbf{x})$
Variance, $V(\mathbf{x})$	$m_2(\mathbf{x}) - (m_1(\mathbf{x}))^2$
Skewness, $S(\mathbf{x})$	$m_3(\mathbf{x}) - 3m_2(\mathbf{x})m_1(\mathbf{x}) + 2(m_1(\mathbf{x}))^3$
Kurtosis, $K(\mathbf{x})$	$m_4(\mathbf{x}) - 4m_3(\mathbf{x})m_1(\mathbf{x}) - 3(m_2(\mathbf{x}))^2 + 12m_2(\mathbf{x})m_1(\mathbf{x})^2 - 6(m_1(\mathbf{x}))^4$

Description of Model

The model used for testing the HOS migration algorithm was a one-dimensional (1-D) model comprising of several homogeneous layers. In order to simplify the examples used, the model was constructed in terms of the traveltimes rather than depth. Since we are concerned with investigating the stack component of migration, the

moveout-corrected data was simulated by convolving AVO CMP seismic data with the source signature. This is described in equations (4.7) and (4.8) below.

$$U(\mathbf{x},t) = R(\mathbf{x},t) = A(t) + B(t) \mathbf{x} + C(t) \mathbf{x}^2 + \eta(\mathbf{x},t) \quad (4.7)$$

$$D(\mathbf{x},t) = U(\mathbf{x},t) * S(t) \quad (4.8)$$

where $U(\mathbf{x},t)$ = AVO CMP seismic data

$\eta(\mathbf{x},t)$ = additive noise

$S(t)$ = source signature

$D(\mathbf{x},t)$ = moveout-corrected data

The parameters A, B and C were chosen using the AVO classification based upon reflection coefficient and offset (Barton and Crider, 1999) as illustrated in Figure 4.1 below.

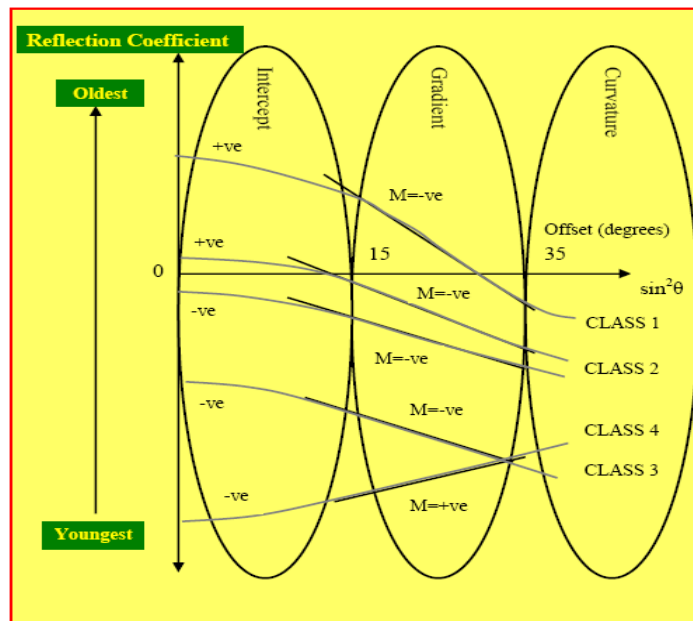


FIGURE 4.1 AVO Classification based upon reflection coefficient and offset (Barton and Crider, 1999).

At specific traveltimes, the events were characterized by different AVO responses. This can be expressed generally by:

$$U_k(\mathbf{x},t) = A_k(t) + B_k(t) \mathbf{x} + C_k(t) \mathbf{x}^2 \quad (4.9)$$

These parameters describing the geological model are shown in Table (4.2) and the AVO CMP seismic data generated for the model are illustrated in Figure 4.2 below.

TABLE 4.2 Parameters defining the geological model used for analysis of new HOS migration algorithm.

PARAMETERS DEFINING GEOMETRY				
A	B	C	TYPE OF AVO RESPONSE	EQUATION DEFINING EACH EVENT
-0.8	0.2	0.0	Linear	$U_1(x,t) = -0.8 + 0.2x$
-0.6	0.15	0.1	Nonlinear	$U_2(x,t) = -0.6 + 0.15x + 0.1x^2$
-0.2	-0.2	0.2	Nonlinear	$U_3(x,t) = -0.2 - 0.2x + 0.2x^2$
-0.05	-0.3	0.3	Nonlinear	$U_4(x,t) = -0.05 - 0.3x + 0.3x^2$
0.05	-0.35	0.0	Linear	$U_5(x,t) = 0.05 - 0.35x$
0.05	-0.35	0.5	Nonlinear	$U_6(x,t) = 0.05 - 0.35x + 0.5x^2$
0.4	-0.55	0.7	Nonlinear	$U_7(x,t) = 0.4 - 0.55x + 0.7x^2$

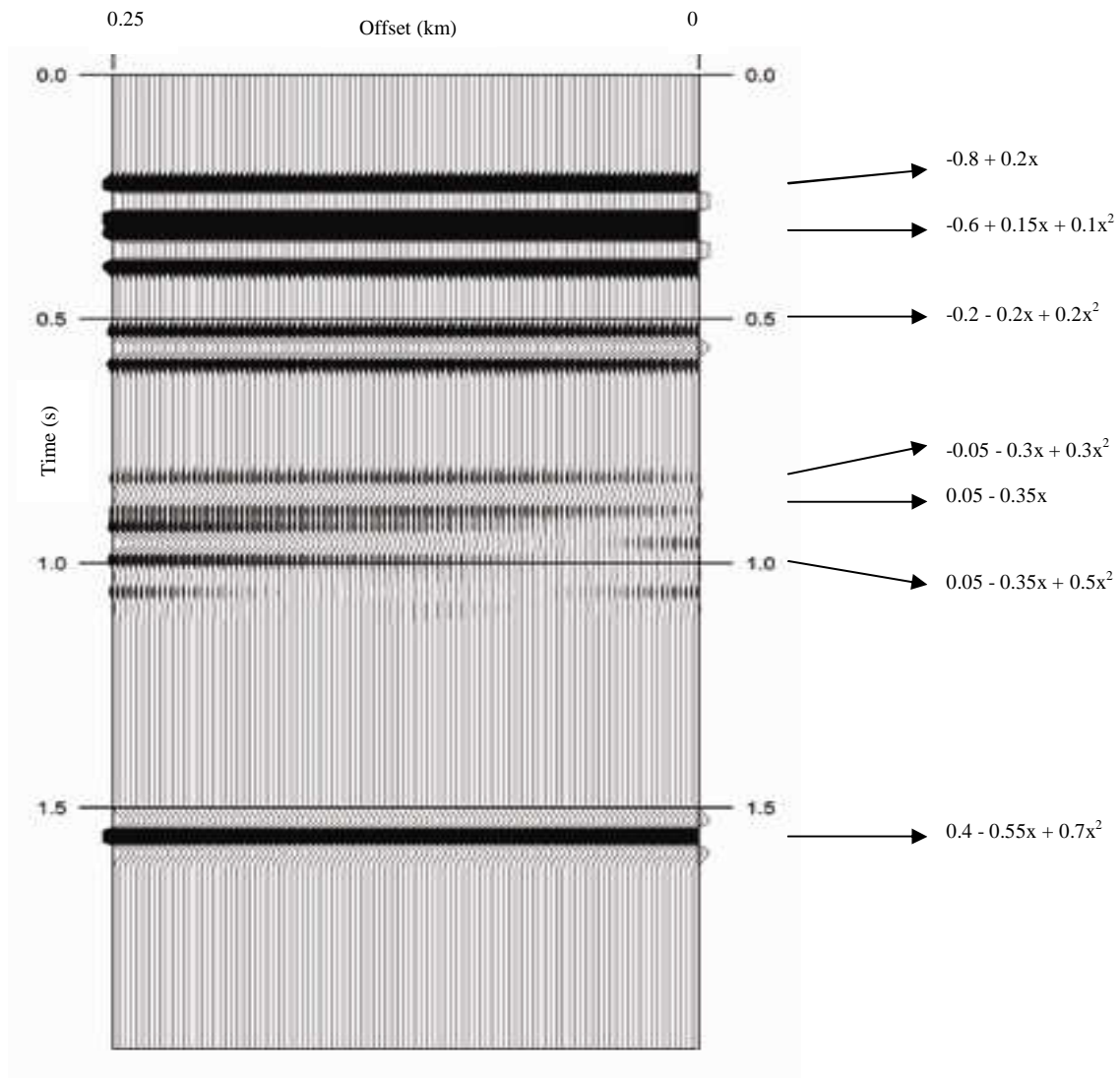


FIGURE 4.2 AVO moveout-corrected seismic data of geological model.

Examples of HOS Migration

For the purposes of this investigation three examples are considered using the geological model described above. In the first example, no noise is added to the events. In the second example, Gaussian noise is added to each event. And in the final example, different types of noise are added to the events. For each case the statistics, i.e. the mean, variance, skewness and kurtosis are computed following the equations defined in Table 4.1. This is illustrated in Figures 4.3 to 4.5 respectively.

Analysis of Results

In the first example (Figure 4.3), no significant noise is added in this case. All layers are well resolved by the mean as one might expect. The variance is quite small in this case. Therefore the plot associated with it may not be that important. However, we can notice that the portion of the data with significant interference produces a large variance. This result is consistent with the fact that the amplitude may vary over a large range in this area. The skewness is zero for the events with linear AVO response. This is so because the data is uniform and therefore symmetric as observed in the previous chapter. Notice that kurtosis is essentially negative in this example, which is consistent with the fact that data without noise tends more to sub-Gaussian.

Now, in the second example (Figure 4.4), we have added Gaussian noise to the data. Basically, the results are essentially unchanged except for the last event which has a large AVO curvature and is therefore non-Gaussian. This combination with Gaussian noise produces a slightly positive kurtosis.

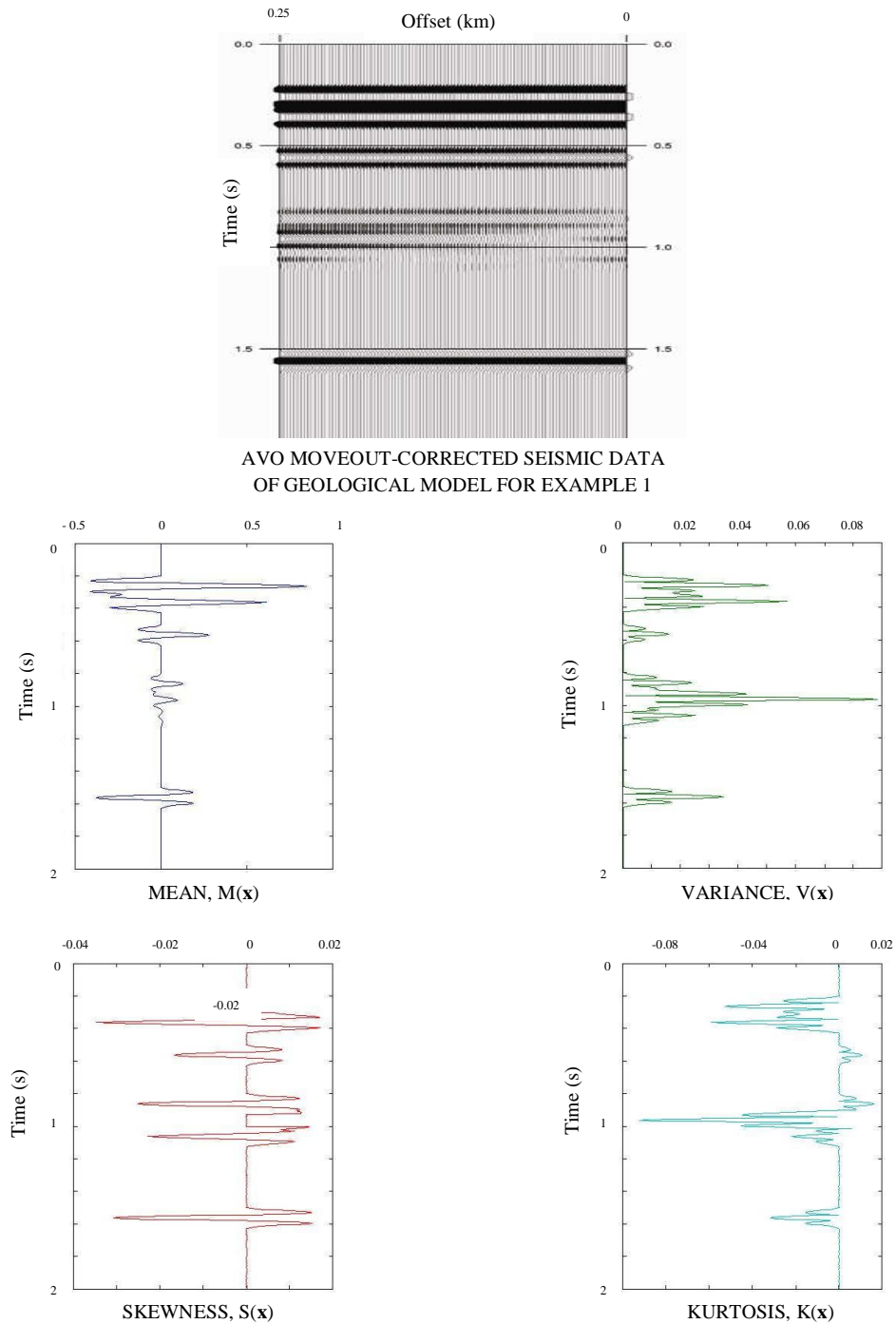
EXAMPLE 1: NO NOISE ADDED

FIGURE 4.3 AVO moveout-corrected seismic data used for example 1 and the corresponding statistical averages.

EXAMPLE 2: GAUSSIAN NOISE ADDED

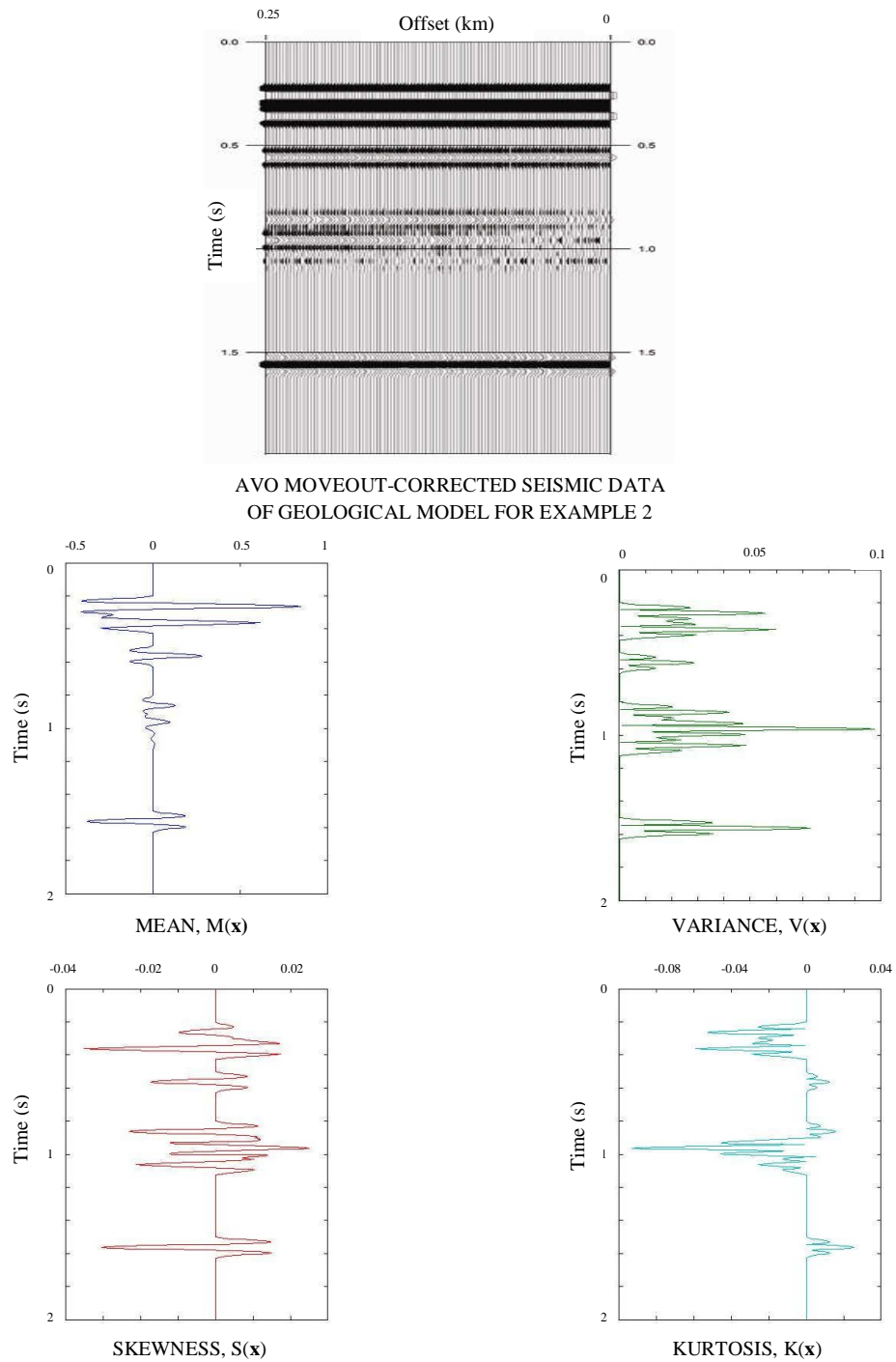


FIGURE 4.4 AVO moveout-corrected seismic data used for example 2 and the corresponding statistical averages.

EXAMPLE 3: DIFFERENT TYPES OF NOISE ADDED

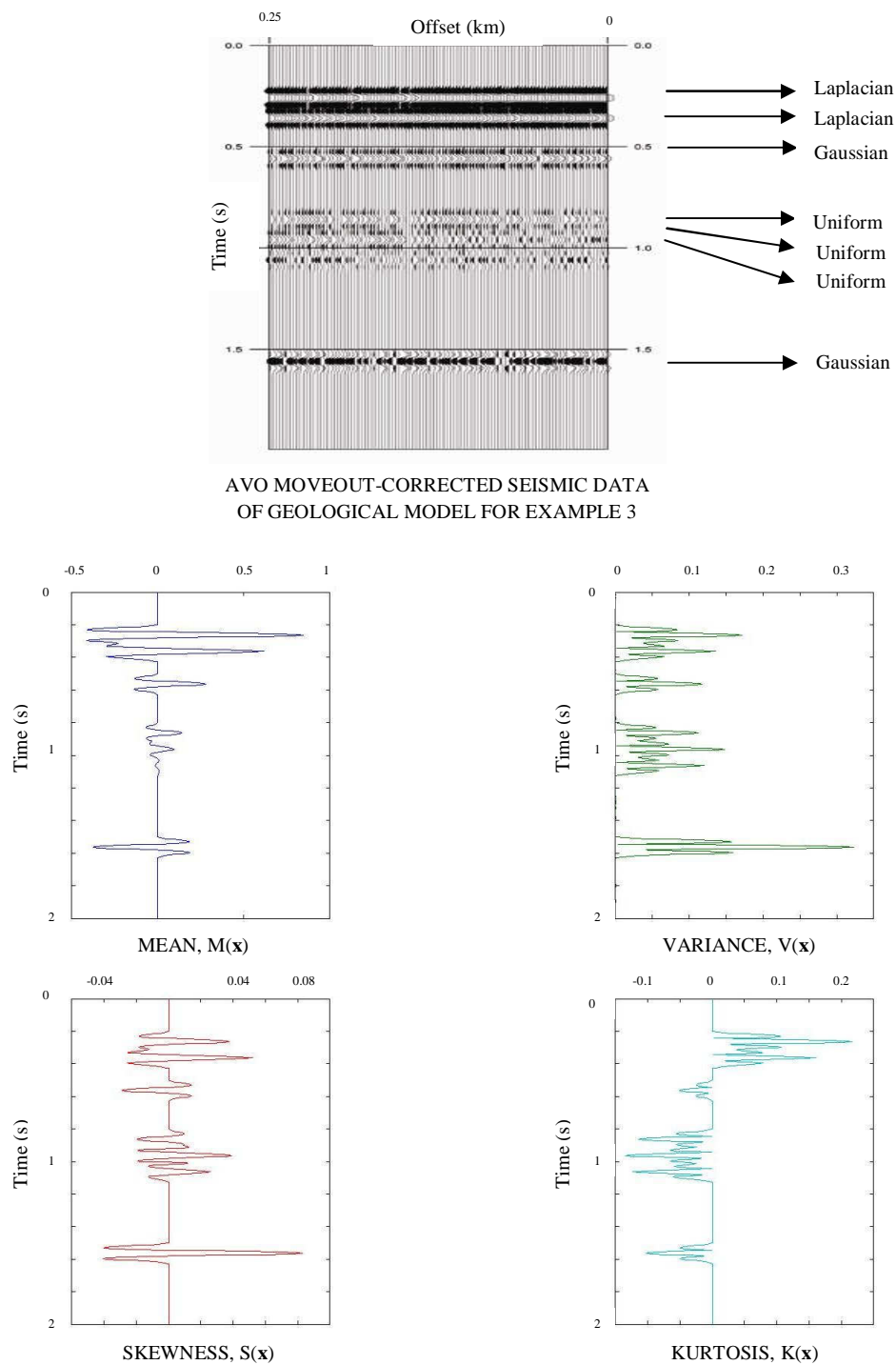


FIGURE 4.5 AVO moveout-corrected seismic data used for example 3 and the corresponding statistical averages.

In the final example (Figure 4.5), we have added different types of noise. The noise component varies with time and includes both Gaussian and non-Gaussian noise, with the non-Gaussian noise being either Uniform or Laplacian. For the first two events in the data, the noise is Laplacian and we can see that the kurtosis has captured well this information with the positive kurtosis (super Gaussian). The middle events with Uniform noise can clearly captured with the negative kurtosis (sub Gaussian). For the last event, we have Gaussian noise and nonlinear AVO behavior. In this case it is still not clear how to define the result which can be sub Gaussian or super Gaussian.

CHAPTER V

SUMMARY AND CONCLUSIONS

The main motivation for the use of HOS in seismic imaging is the fact that many signals in real life cannot be accurately modeled using the traditional 2nd order measures. How accurately seismic imaging can be done depends on both the quality of the sensing equipment and also very much on the effectiveness of the mathematical algorithms that are used. Hence it is important when seismic imaging algorithms are improved.

If seismic modeling and imaging are to be improved, then more of the information available in the data must be extracted and used. The examples presented confirm that extra information carried by HOS can be obtained using my algorithm over conventional imaging algorithms.

The mean attribute produces the same results as the present imaging technique known as stack, whereas variance, skewness and kurtosis allow us to detect and characterize linear and non-linear AVO behavior and the non-Gaussianity of the data.

Using skewness and kurtosis allows for the identification of the transition from Gaussianity to non-Gaussianity, which coincides with the onset of the seismic event despite noise presence. Skewness and kurtosis establish an effective statistical test in identifying signals with asymmetrical distributions and nonlinear AVO behavior. The simplicity of the method makes it an attractive candidate for huge seismic data assessment in a real time context.

Another important conclusion is that there is a significant improvement in the computation time, accuracy and the cost of seismic data processing, because the single

algorithm allows for the output of three parameters, the variance, skewness and kurtosis, simultaneously and because we are avoiding errors associated with converting offsets to angles when analyzing the AVO behavior. Furthermore, we will also be improving the resolution of the seismic data since knowledge of the reflection angles is not necessary to retrieve AVO information.

Hence it is recommended that HOS be employed as a tool in the assessment of seismic data during the processing stage in seismic imaging.

REFERENCES

- Ikelle, L.T., and Amundsen, L., 2005, Introduction to Petroleum Seismology: Society of Exploration Geophysicists, Tulsa, OK.
- Singh, S. K., 2005, Subsalt Imaging: Modeling and Demultiple: M.S.Thesis, Texas A&M University, College Station, TX.
- Watts A. 2005, Linear Demultiple Solution based on Bottom-Multiple Generator (BMG) Reflector Approximation: Subsalt Example: M.S.Thesis, Texas A&M University, College Station, TX.

Supplemental Sources consulted

- Keary, P., and Brooks, M., 1991, An Introduction to Geophysical Exploration: Blackwell Scientific Publications, Oxford.
- Papoulis A. and Pillai S. U., 2002, Probability, Random Variables and Stochastic Processes, 4th Edition, McGraw Hill, New York.
- Srinivasan, K., 1999, Seismic Imaging Using Higher Order Statistics: M.S. Thesis, Texas A&M University, College Station, TX.
- Evans, B. J., 1997, A Handbook for Seismic Data Acquisition in Exploration: Society of Exploration Geophysicists, Tulsa, OK.
- Yilmaz, O., 1987, Seismic Data Processing Series: Society of Exploration Geophysicists, Tulsa, OK.

APPENDIX A

RANDOM VARIABLES, MOMENTS AND CUMULANTS

Random Variables

Random variables are mathematical quantities that are used to represent probabilistic uncertainty. A random variable x is can be described completely by a domain of values and a function (probability distribution or probability density function, pdf) p , or equivalently, by an expectation value function, $E\{.\}$ such that

$$E\{x\} = \int_{-\infty}^{\infty} x \cdot p(x) dx$$

Random variables can also be characterized by the characteristic function. This characteristic function can be defined by

$$\Psi(\omega) = \int_{-\infty}^{\infty} e^{i\omega x} p(x) dx = E(e^{i\omega x})$$

where $e^{i\omega x}$ can be expanded as a Taylor series. The second characteristic function which is also commonly used, is defined by

$$\Psi(\omega) = \ln \Phi(\omega)$$

Moments

When summarizing certain properties of a random variable by using expectations of the random variable to some power, these expectations can be described as moments.

The k^{th} moment m_k of a random variable x is given by

$$m_k = E\{x^k\} = \int_{-\infty}^{\infty} x^k p(x) dx$$

Using this definition of moments, i.e. $m_k = E\{x^k\}$, and that of the first characteristic function defined in equation (2.2), we obtain

$$\Phi(\omega) = \sum_{k=0}^{\infty} m_k (i\omega)^k$$

Hence the moments can be derived by the differentiation of the characteristic function, such that

$$m_k = i^{-k} \frac{d^k \Phi(\omega)}{d\omega^k}$$

If $\eta = E\{x\}$ is the first order statistical moment (the *mean* or average value of the random variable), the k^{th} central moment is defined as

$$\mu_k = E\{(x - \eta)^k\} = \int_{-\infty}^{\infty} (x - \eta)^k p(x) dx$$

Clearly, $m_0 = \mu_0 = 1$, $m_1 = \eta$ and $\mu_1 = 0$.

Cumulants

Cumulants can also be used to describe random variables. They allow Gaussian and non-Gaussian random variables to be distinguished much easier than moments. The cumulants c_k are defined by the cumulant-generating function

$$g(\omega) = \log(E(\exp(\omega X))) = \sum_{k=1}^{\infty} c_k \frac{\omega^k}{k!} = \mu\omega + \frac{\omega^2}{2} + \dots$$

The moment-generating function is given by

$$1 + \sum_{k=1}^{\infty} c_k \frac{\omega^k}{k!} = \exp\left(\sum_{k=1}^{\infty} \frac{\omega^k c_k}{k!}\right) = \exp(g(\omega))$$

The cumulant-generating function is the logarithm of the moment generating function.

The cumulants are given by derivatives (at zero) of $g(\omega)$

$$c_k = g^{(k)}(0)$$

e.g. $c_1 = \mu = g'(0)$, $c_2 = \sigma^2 = g''(0)$

The cumulants of a distribution are closely related to distribution's moments. The first cumulant is the expected value; the second and third cumulants are respectively the second and third central moments (the second central moment is the variance); but the higher cumulants are neither moments nor central moments, but rather more complicated polynomial functions of the moments. Working with cumulants can have an advantage over using moments because for independent variables X and Y,

$$g_{X+Y}(\omega) = \log(E(e^{\omega(X+Y)})) = \log(E(e^{\omega X})) \cdot \log(E(e^{\omega Y})) = \log(E(e^{\omega X})) + \log(E(e^{\omega Y}))$$

i.e.
$$g_{X+Y}(\omega) = g_X(\omega) + g_Y(\omega)$$

so that each cumulant of a sum is the sum of the corresponding cumulants of the addends. More generally, we can rewrite equation (x) as:

$$c_k(X + Y) = c_k(X) + c_k(Y)$$

This property of cumulants is known as additivity.

A more formal definition of the cumulants can be given in terms the second characteristic function of a probability distribution, as defined above. Similar to moments,

$$\Psi(\omega) = \sum_{k=0}^{\infty} c_k (i\omega)^k$$

The cumulants c_k can therefore be defined by the relation,

$$c_k = i^{-k} \frac{d^k \ln \Phi(\omega)}{d\omega^k}$$

Variance, Skewness, Kurtosis

The *variance* or dispersion of a distribution indicates the spread of the distribution with respect to the mean value. It can be defined as follows:

$$\sigma^2 = E\{(x - \eta)^2\} = \int_{-\infty}^{\infty} (x - \eta)^2 p(x) dx$$

A lower value of variance indicates that the distribution is concentrated close to the mean value, and a higher value indicates that the distribution is spread out over a wider range of possible values.

The *skewness* of a distribution indicates the asymmetry of the distribution around its mean, characterizing the shape of the distribution. It is given by

$$\gamma_1 = \frac{1}{\sigma^3} E\{(x - \eta)^3\} = \frac{1}{\sigma^3} \int_{-\infty}^{\infty} (x - \eta)^3 p(x) dx$$

The distribution, i.e. dataset, is symmetric if it looks the same to the left and right of the peak point. The skewness for a normal distribution is zero and any symmetric data should also have skewness near zero. A positive value of skewness indicates that the distribution is skewed towards values greater than the mean (i.e., skewed towards the

right side) and a negative value indicates that the distribution is skewed towards the left side.

The *kurtosis* of a distribution indicates the flatness of the distribution with respect to the normal distribution. It is given by

$$\gamma_2 = \frac{1}{\sigma^4} E\{(x-\eta)^4\} = \frac{1}{\sigma^4} \int_{-\infty}^{\infty} (x-\eta)^4 p(x) dx$$

Positive kurtosis indicates a peaked distribution, whereas negative kurtosis indicates a flat distribution. Distributions with positive kurtosis are sometimes termed super Gaussian and distributions with negative kurtosis are sometimes termed sub Gaussian. Kurtosis can be considered a measure of the non-Gaussianity of the random variable, x . For a Gaussian random variable, kurtosis is zero, for a uniform distribution it is negative and for a Laplace distribution it is positive.

VITA

Name: Janelle Greenidge

Address: #4 Eighth Street West
Cassleton Avenue, Trincity
Trinidad, W.I.

Email: jcgreenidge@hotmail.com

Education: M.S., May 2008
Texas A&M University
Department of Geology and Geophysics
Thesis: Seismic Attribute Analysis Using Higher Order Statistics
Major: Geophysics

B.S., August 2000
University of the West Indies
Department of Physics
Research Project: Electroencephalography for Left Handed Persons
Major: Physics

Postgraduate Diploma, October 2004
University of the West Indies
Department of Chemical Engineering
Petroleum Engineering Unit
Major: Petroleum Engineering